

1  
2  
3  
4  
5  
6  
7  
8  
9  
10  
11  
12  
13  
14  
15  
16  
17  
18  
19  
20  
21  
22  
23  
24  
25  
26  
27  
28  
29  
30  
31  
32  
33  
34  
35  
36

## REVISION 2

### TITLE

# CRYSTAL CHEMISTRY AND LIGHT ELEMENTS ANALYSIS OF Ti-RICH GARNETS

Schingaro Emanuela<sup>1</sup>, Lacalamita Maria<sup>1\*</sup>, Mesto Ernesto<sup>1</sup>, Ventruti Gennaro<sup>1</sup>, Pedrazzi  
Giuseppe<sup>2</sup>, Ottolini Luisa<sup>3</sup>, Scordari Fernando<sup>1</sup>

<sup>1</sup>Dipartimento di Scienze della Terra e Geoambientali, Università degli Studi di Bari “Aldo Moro”,  
via E. Orabona 4, I-70125, Bari, Italy

<sup>2</sup>Dipartimento di Neuroscienze, Università di Parma, via Volturno 39, I-43100, Parma, Italy

<sup>3</sup>CNR-Istituto di Geoscienze e Georisorse, Unità di Pavia, via A. Ferrata 1, I-27100 Pavia, Italy

submitted to: *American Mineralogist*

address of the corresponding author:

Prof. Emanuela Schingaro

Dipartimento di Scienze della Terra e Geoambientali,

Università degli Studi di Bari “Aldo Moro”

Via Orabona 4, I-70125 Bari, Italy

Phone 0039-080-5443578

e-mail: [emanuela.schingaro@uniba.it](mailto:emanuela.schingaro@uniba.it)

37

38

## ABSTRACT

39

A suite of Ti-bearing garnets from magmatic, carbonatitic and metamorphic rocks was

40

studied by Electron Probe Microanalysis (EPMA), X-ray Powder Diffraction (XRPD), Single

41

Crystal X-ray Diffraction (SCXRD), Mössbauer spectroscopy and Secondary Ion Mass

42

Spectrometry (SIMS) in order to better characterize their crystal chemistry. The studied garnets

43

show TiO<sub>2</sub> varying in the ranges 4.9(1) - 17.1(2) wt% and variable Fe<sup>3+</sup>/ΣFe content. SIMS analyses

44

allowed quantification of light elements yielding H<sub>2</sub>O in the range 0.091(7) - 0.46(4), F in the range

45

0.004(1) - 0.040(4) and Li<sub>2</sub>O in the range 0.0038(2) - 0.014(2) wt%. Mössbauer analysis provided

46

spectra with different complexity, which could be fitted to a number of components variable from

47

one (<sup>Y</sup>Fe<sup>3+</sup>) to four (<sup>Y</sup>Fe<sup>2+</sup>, <sup>Z</sup>Fe<sup>2+</sup>, <sup>Y</sup>Fe<sup>3+</sup>, <sup>Z</sup>Fe<sup>3+</sup>). A good correlation was found between the Fe<sup>3+</sup>/ΣFe

48

resulting from the Mössbauer analysis and that derived from the Flank method.

49

X-ray powder analysis revealed that the studied samples are a mixture of different garnet

50

phases with very close cubic unit cell parameters as recently found by other authors. Single crystal

51

X-ray refinement using anisotropic displacement parameters were performed in the  $Ia\bar{3}d$  space

52

group and converged to  $1.65 \leq R_1 \leq 2.09$  % and  $2.35 \leq wR_2 \leq 3.02$  %. Unit cell parameters vary in

53

the range  $12.0641(1) \leq a \leq 12.1447(1)$  Å, reflecting different Ti contents and extent of substitutions

54

at tetrahedral site.

55

The main substitution mechanisms affecting the studied garnets are:  ${}^Y\text{R}^{4+} + {}^Z\text{R}^{3+} \leftrightarrow {}^Z\text{Si} +$

56

${}^Y\text{R}^{3+}$  (schorlomite substitution);  ${}^Y\text{R}^{2+} + {}^Z\text{R}^{4+} \leftrightarrow 2{}^Y\text{R}^{3+}$  (morimotoite substitution);  ${}^Y\text{R}^{3+} \leftrightarrow {}^Y\text{Fe}^{3+}$

57

(andradite substitution); in the above substitutions  ${}^Y\text{R}^{2+} = \text{Fe}^{2+}, \text{Mg}^{2+}, \text{Mn}^{2+}$ ;  ${}^Z\text{R}^{4+} = \text{Ti}$ ;  ${}^Y\text{R}^{3+} = \text{Fe}^{3+},$

58

$\text{Al}^{3+}, \text{Cr}^{3+}$ ;  ${}^Z\text{R}^{3+} = \text{Fe}^{3+}, \text{Al}^{3+}$ . Minor substitutions, such as  $2{}^Y\text{Ti}^{4+} + {}^Z\text{Fe}^{2+} \leftrightarrow 2{}^Y\text{Fe}^{3+} + {}^Z\text{Si}, (\text{SiO}_4)^{4-} \leftrightarrow$

59

$(\text{O}_4\text{H}_4)^{4-}, \text{F}^- \leftrightarrow \text{OH}^-$  and  ${}^Y\text{R}^{4+} + {}^X\text{R}^+ \leftrightarrow {}^Y\text{R}^{3+} + {}^X\text{Ca}^{2+}$ , with  ${}^Y\text{R}^{4+} = \text{Ti}, \text{Zr}$ ;  ${}^Y\text{R}^{3+} = \text{Fe}^{3+}, \text{Al}, \text{Cr}^{3+}$ ;  ${}^X\text{R}^+$

60

= Na, Li also occur.

61

62

63

64 **Keywords:** Ti-bearing garnets, light elements, SCXRD, XRPD, EPMA, SIMS, Mössbauer

65 spectroscopy, crystal chemistry.

66

67

68

69

70

71

72

73

74

75

76

77

78

79

80

81

82

83

84

85

86

87

88

89

90

91

92

93

## INTRODUCTION

Garnets are a supergroup of rock-forming minerals, with generalized chemical formula  $\{X_3\}[Y_2](Z_3)\phi_{12}$  where dodecahedral  $\{X\}$ , octahedral  $[Y]$  and tetrahedral  $(Z)$  are the three symmetrically unique atomic sites and the anionic site ( $\phi$ ) represents  $O^{2-}$ ,  $OH^-$ , and  $F^-$  (Grew et al. 2013). Alternating  $Z\phi_4$  tetrahedra and  $Y\phi_6$  octahedra share corners to form a three-dimensional framework containing  $X\phi_8$  triangular dodecahedra.

These minerals are widespread in the Earth's crust, upper mantle and transitional zone and occur in a variety of rocks. In a recent revision of the nomenclature of garnets (Grew et al. 2013), thirty-two species of the garnet supergroup were approved, out of which twenty-nine were further divided into five groups, on the basis of the symmetry and of the total charge of cations at the tetrahedral site: henritermierite (tetragonal, Z charge = 8), bitikleite (cubic, Z charge = 9), schorlomite (cubic, Z charge = 10), garnet (cubic, Z charge = 12), berzellite (cubic, Z charge = 15). Ti-garnets may belong to the schorlomite or to the garnet group, depending on the composition and cation distribution (see below). In previous literature, Ti-garnets are referred to as Ti-bearing andradite, melanite, schorlomite and morimotoite, and Chakhmouradian and McCammon (2005) reviewed the criteria historically used to distinguish between melanite and schorlomite. From a geological viewpoint, Ti-rich garnets are found in various silica undersaturated alkaline igneous rocks (Huggins et al. 1977a, 1977b; Dingwell and Brearley 1985; Gwalani et al. 2000; Saha et al. 2011) and are related to alkali metasomatism and magmatism of carbonatitic affinity (Platt and Mitchell 1979; Deer et al. 1982).

Depending on the species occupying the crystallographic sites, they may be used as tracers of magma evolution (Lupini et al. 1992; Gwalani et al. 2000; Brod et al. 2003), as indicators of  $f_{O_2}$ ,  $f_{H_2O}$  and other thermodynamic parameters active during the mineral crystallization. In addition, their crystal chemistry is recognized to affect the partitioning of trace elements between the garnets and

118 the melt, and this information can be used to constrain petrogenetic processes in planetary interiors  
119 (Dwarzski et al. 2006).

120         However, the determination of the correct crystal chemistry of garnets is very complex  
121 because of the great number of substituting cations over the three independent crystallographic sites  
122 and, with particular regards to Ti-rich garnets, of the multiple oxidation states and coordination  
123 environments of transition elements such as Fe and Ti. This topic has been thoroughly reviewed by  
124 Grew et al. (2013), also in view of the relevant implications for classification and nomenclature of  
125 garnets.

126         Ti-garnets may also incorporate hydrogen, fluorine, lithium in trace but measurable  
127 amounts. In particular, the OH-bearing garnets may be a reservoir of hydrogen in the Earth's mantle  
128 and may also affect the evolution of the hydrosphere through its influence on mantle melting and  
129 isotopic fractionation (Bell et al. 2004).

130         Quantitative analysis of trace hydrogen is therefore necessary for a better understanding of  
131 its role in geological processes but, unfortunately, there is no routinary method to obtain this  
132 information. For instance, the hydrogen content (conventionally quantified as H<sub>2</sub>O, wt%) in  
133 schorlomes and Ti-andradites was often estimated from the summed integrated OH<sup>-</sup> absorbance in  
134 the infrared spectra using a wavenumber-dependent calibration (Lager et al. 1989; Müntener and  
135 Hermann 1994; Locock et al. 1995; Amthauer and Rossman 1998; Katerinopoulou et al. 2009;  
136 Phichaikamjornwut et al. 2011). Actually, it has been demonstrated that the choice of a calibration  
137 method for garnets is not unambiguous since considerable discrepancies exists among the available  
138 calibrations (e.g., Maldener et al. 2003). The hydrogen content of titanian andradites from  
139 Sanbagawa metamorphic rocks (Central Japan), melilitic rocks of the Osečná complex (Bohemia)  
140 and schorlomes from Afrikanda (Kola Peninsula) silicocarbonatite was measured respectively by  
141 means of wet analysis, gravimetry and combustion (Onuki et al. 1982; Ulrych et al. 1994;

142 Chakhmouradian and McCammon 2005). Kühberger et al. (1989) used the solid's moisture analyzer  
143 to determine the water content in synthetic Ti-andradite.

144 Multiple mechanisms have been proposed to describe the hydrogen uptake in garnets. The  
145 hydrogarnet substitution ( $4\text{H} + \text{Z}[\text{O}] \rightarrow [\text{O}] + \text{ZSi}$ ), where, i.e., a  $\text{SiO}_4$  unit may be replaced by  $\text{H}_4\text{O}_4$  on  
146 the tetrahedral site, was often invoked because consistent with diffraction technique data from H-  
147 rich samples (e.g., Lager et al. 1987, 1989; Eeckhout et al. 2002; Ferro et al. 2003). Evidences from  
148 electron microprobe data, nuclear magnetic resonance (NMR) and infrared (IR) spectra have been  
149 reported as pointing to octahedral and dodecahedral hydrogen occupancy in garnets (Basso et al.  
150 1984a, b; Kalinichenko et al. 1987; Basso and Cabella 1990; Rossman and Aines 1991).

151 Fluorine content of Ti-andradites or titanium andradites-grossular was mainly obtained by  
152 electron-microprobe analysis (Flohr and Ross 1989; Manning and Bird 1990; Barbanson and Bastos  
153 Neto 1992; Visser 1993; Ulrych et al. 1994; Freiburger et al. 2001; Faryad and Dianiška 2003) but  
154 also by F-sensitive glass electrode (Armbruster et al. 1998). Exchange reaction  $\text{F}^- \leftrightarrow \text{OH}^-$  was used  
155 to explain the incorporation of fluorine in garnet, but also more complex reactions were proposed  
156 involving coupled cations substitutions for charge balance (Valley et al. 1983).

157 To the best of our knowledge, studies on lithium in Ti-garnets, instead, are missing in  
158 literature. For natural or synthetic Ti-free, Li-rich garnets it was proposed that lithium occupies not  
159 only the Z but also the Y, X and interstitial 96h sites (Cussen 2006; Cempírek et al. 2010). These  
160 garnets have high-ionic conductivity (e.g. Wang and Lai 2012) or notable implications as a  
161 geobarometer (Yang et al. 2009).

162 In the present study, hydrogen, fluorine and lithium were measured in a suite of Ti-garnets  
163 from a variety of rock types by means of secondary ion mass spectrometry (SIMS). This technique  
164 was only previously used to derive an  $\text{H}_2\text{O}$  calibration curve employing, however, garnets with  
165 pyralspite composition, whose hydrogen abundance were determined by manometry and IR  
166 measurements (Koga et al. 2003).

167 The results of SIMS, electron microprobe analysis (EPMA), X-ray powder diffraction  
168 (XRPD), single crystal X-ray diffraction (SCXRD) and Mössbauer spectroscopy have been here  
169 integrated in the present study of Ti garnets of different origin and provenance in order to provide a  
170 comprehensive crystal chemical characterization of the studied samples.

171

172

## MATERIALS AND METHODS

### 173 Samples

174 The analysed samples are from different geologic environments: magmatic alkaline,  
175 carbonatitic and metamorphic rocks. The details of samples origin and provenance are reported in  
176 **Table 1**. Most of the analysed samples have been previously partially characterized and the relevant  
177 results published in the papers reported in the last column of **Table 1**. In the present work, for the  
178 first time a full crystal chemical characterization is accomplished for W6 and W16 samples. In  
179 addition, a re-examination of the crystal chemical formulae of W12, NZALA and ZER2 samples,  
180 previously studied by some of the authors, is here proposed on the basis of EPMA, SIMS, XRPD  
181 and SCXRD measurements on new crystals. Non routinary chemical analysis (EPMA with the  
182 Flank method, SIMS see below) are reported for the first time on the whole suite of study samples  
183 as well as the results of XRPD measurements.

184

### 185 EPMA

186 Quantitative elemental analyses of the studied crystals (embedded in epoxy resin and  
187 polished) were performed with a JEOL JXA-8200 electron microprobe (Dipartimento di Scienze  
188 della Terra, University of Milano) operating at 15 kV acceleration voltage, 5 nA beam current, ~ 1  
189  $\mu\text{m}$  beam size and 30s counting time. All the elements were analysed in wavelength dispersive  
190 spectrometry (WDS) mode and the adopted standards were: wollastonite (Si), anorthite (Al, Ca),  
191 olivine (Mg), fayalite (Fe), omphacite (Na), ilmenite (Ti), Cr pure (Cr), rhodonite (Mn) and zircon

192 jarosite (Zr). A Phi-Rho-Z routine as implemented in the JEOL suite of programs was used for the  
193 matrix correction. Analytical measurements were affected by a relative uncertainty of 1% for major  
194 elements and 4% for minor elements. ‘Flank method’ measurements for the determination of the  
195  $\text{Fe}^{3+}/\Sigma\text{Fe}$  were carried out with the same electron microprobe as above, in WDS mode, employing a  
196 TAP crystal and a 300  $\mu\text{m}$  slit.  $\text{FeL}\beta$  and  $\text{FeL}\alpha$  peaks were searched and measured for counting  
197 times of 300 s. The correction for self-absorption was applied (Höfer and Brey 2007) and natural  
198 and synthetic garnet end-members with fixed  $\text{Fe}^{3+}/\Sigma\text{Fe}$  were used as standards (Malaspina et al.  
199 2009). The accuracy of the Flank method has been defined by a maximum error of  $\pm 0.04$  for  
200  $\text{Fe}^{3+}/\Sigma\text{Fe}$  in samples with total Fe in the range 8-11 wt % (Höfer and Brey 2007).

201

## 202 SIMS

203 SIMS analyses were performed with the ion microprobe Cameca IMS 4f installed at CNR-  
204 IGG (Pavia) following procedures similar to those reported in Ottolini et al. (1995, 2002). A static,  
205 mass filtered  $^{16}\text{O}^-$  primary beam accelerated to 12.5 kV was focused on the sample surface to obtain  
206 a current intensity of 9.5 nA, corresponding to  $\sim 15 \mu\text{m}$  beam diameter. The second aperture (400  
207  $\mu\text{m}$   $\emptyset$ ) on the primary-beam selector was used to prevent  $^{16}\text{O}^1\text{H}^-$  ions, which forms a weak second  
208 spot on the sample (clearly visible in anhydrous samples), from reaching the ion probe sample  
209 chamber (SC). Positive secondary ions from the sample were extracted by a 4.5 kV accelerating  
210 voltage and transferred into the mass spectrometer by the 25  $\mu\text{m}$  secondary-ion optics. Secondary  
211 ions were “energy filtered” with an emission energy in the range  $\sim 75$ -125 eV.  $\text{H}^+$ ,  $^7\text{Li}^+$ ,  $^{19}\text{F}^+$  and  
212  $^{30}\text{Si}^+$  ion signals were detected after 450-sec waiting time required to get steady-state sputtering  
213 conditions. Acquisition times were 3s for  $\text{H}^+$  and  $^7\text{Li}^+$  each, 8s for  $^{19}\text{F}^+$  and 3s for  $^{30}\text{Si}^+$  for each of  
214 the two analytical cycles. Hydrogarnet crystals and standards were left to degas seven days in the  
215 ion probe SC before running analysis. Detection limits for H ( $6\sigma$  background) were estimated on the  
216 order of 20 ppm H.

217 The results for H, Li and F were put on a quantitative basis using empirical calibration  
218 curves based on standards that were the following: schorl (no. 16), dravite (no. 18), elbaite (no. 19),  
219 fully characterized in Ottolini et al. (2002). In particular, for H quantification we used the  
220 extrapolated regression line:  $IY(H/Si)$  vs.  $(Fe_{tot}+Ti+Mn)(at)$ , first derived in kornerupine (Ottolini  
221 and Hawthorne 2001) and then successfully tested in several silicate matrixes (see for instance,  
222 Scordari et al. 2010 and reference therein). The analytical accuracy for Li is on the order of 5%  
223 relative. An accuracy of better than 10% relative is quoted for H and F.

224

### 225 **Mössbauer spectroscopy**

226 Mössbauer spectra were recorded on powdered samples (~ 10 mg) at room temperature, in  
227 transmission geometry, using a source of  $^{57}Co/Rh$  matrix (~ 1GBq) and a constant acceleration  
228 spectrometer. Spectra were recorded using a multichannel analyzer (1024 or 512 channels) in the  
229 velocity range  $\pm 4$  mm/s and subsequently folded (Shenoy et al. 1978). More than  $10 \times 10^6$  baseline  
230 counts per channel were recorded for each spectrum. Isomer shifts (IS) are expressed relative to  $\alpha$ -  
231 iron. The spectra were fitted with routines employing Levenberg-Marquardt methods and  
232 implemented in the software RECOIL 1.03a (Lagarec and Rancourt 1997, 1998).

233

### 234 **XRPD**

235 X-ray powder diffraction patterns were recorded using a Panalytical Empyrean  
236 diffractometer equipped with a PIXcel-3D detector.  $Cu K\alpha$  radiation ( $\lambda = 1.5418 \text{ \AA}$ ) was employed  
237 and the instrument operated at 40 kV/40 mA. Because of the shortage of samples, powders were  
238 loaded in a zero background silicon sample holder and slightly compressed with a glass slide. The  
239 patterns were collected in the  $2\theta$  range of  $5^\circ$ - $140^\circ$ . The divergence and antiscatter slits were 1/8 and  
240  $\frac{1}{4}$  mm, respectively, and the detector slit was 7.5 mm. Qualitative phase analysis was performed by  
241 means of the PANalytical HighScore software. Quantitative analysis and the refinement of the

242 lattice parameters were carried out by the Rietveld Method (Young 1993) as implemented in the  
243 GSASII software (Toby and Von Dreele 2013).

244

## 245 **SCXRD**

246 Single crystal X-ray diffraction data were collected using a Bruker AXS X8 APEXII  
247 automated diffractometer (Dipartimento di Scienze della Terra e Geoambientali, University of Bari)  
248 with a charge coupled device (CCD) detector and a four-circle Kappa goniometer. The X-ray data  
249 were acquired using a graphite monochromatized MoK $\alpha$  radiation, several  $\omega$  and  $\phi$  rotation scans,  
250 1.0° scan width, 10 s per frame exposure time, crystal-to-detector distance of 40 mm and operating  
251 conditions of 50 kV and 30 mA. The COSMO program of the Apex program suite (Bruker 2003a)  
252 was used to optimize the data collection strategy whereas for cell determination and data reduction  
253 the SAINT (Bruker 2003b) and SADABS programs (Sheldrick 2003) were employed. Least-squares  
254 refinements were performed using the program CRYSTALS (Betteridge et al. 2003) in the space  
255 group  $Ia\bar{3}d$ . Scale factor, atomic positions, cation occupancies and anisotropic displacement factors  
256 were refined. Fully ionized scattering factors were used. Since compositional disorder can affect all  
257 three independent sites in the garnet structure (see the **Introduction** section) different cation  
258 distribution were tested in order to obtain the best fit between mean atomic numbers estimated via  
259 EPMA and structure refinement (X-ref). Preliminary refinements allowed to ascertain that  
260 tetrahedral site occupancy could assume values less than 1, indicating the occurrence of tetrahedral  
261 vacancies. In addition, the refined tetrahedral mean atomic number could be less or greater than  
262 14e<sup>-</sup>, indicating respectively the presence of a lighter or a heavier substituent of Si atoms. Also Ca  
263 occupancy was initially left free to vary to check for the occurrence of Fe<sup>2+</sup> at X (in this case the  
264 mean atomic number would refine to more than 20 e<sup>-</sup>). In final refinements, depending of the bulk  
265 chemistry of each sample, the following refinement restrictions (Watkin 2008) were used:

- 266 1) at the X-site, the occupancy of Ca was constrained so that the site was fully occupied;  
267 2) at the Y-site, the Al and Fe occupancies (with Fe representing Mn + Ti (+ Zr) and Al  
268 representing Mg scattering species) were restrained to obtain a full occupancy;  
269 3) at the Z-site, the Si (standing also for Al), or Si and Fe occupancies were refined with a restraint  
270 which could result in a total occupancy less, equal or greater than 1. The only exception was for  
271 sample ZER2: in this case Si occupancy was constrained to be 1.

272

273

## RESULTS AND DISCUSSION

### 274 Chemical composition

275 EPMA data calculated as average over 4-10 spots are reported in **Table 2** together with  
276 SIMS data. Indeed, the within grain coefficient of variation (CV) is < 10% for all the measured  
277 oxides with the exception of Na<sub>2</sub>O, ZrO<sub>2</sub>, Cr<sub>2</sub>O<sub>3</sub>, whereas as far as light elements are concerned, it  
278 is ~ 10% for H<sub>2</sub>O, generally > 50% for Li<sub>2</sub>O and variable (4-44%) for the F content.

279 In particular, the studied Ti-garnets are characterized by variable degree of hydration. SIMS  
280 analyses provide H<sub>2</sub>O concentration in the range 0.091(7)-0.46(4) wt% (**Table 2**) which is in  
281 agreement (see also **Figure 1**) with the values measured for most of the Ti-garnets with andradite,  
282 andradite-grossular, andradite-uvarovite or schorlomite component (Müntener and Hermann 1994;  
283 Locock et al. 1995; Amthauer and Rossman 1998; Chakhmouradian and McCammon 2005;  
284 Katerinopoulou et al. 2009; Phichaikamjornwut et al. 2011). However, higher H<sub>2</sub>O contents (from  
285 1.25 to 2.90 wt%) were reported for other Ti-garnets (Onuki et al. 1982; Lager et al. 1989; Ulrych et  
286 al. 1994; Amthauer and Rossman 1998). Galuskin (2005) calculated, on the basis of charge balance,  
287 ~ 5 wt% H<sub>2</sub>O in the “hydroschorlomite” whereas up to 10 wt% H<sub>2</sub>O was estimated from cell  
288 dimensions considerations in the “hydroandradite” (Armbruster 1995).

289 Very low amount of Li<sub>2</sub>O (0.0038(2) - 0.014(2) wt%) equivalent to 0.001-0.005 atoms per  
290 formula unit was detected in the studied samples (**Table 2**). These values are similar to those (0-

291 0.004 apfu) found in Ti-free garnets (Grew et al. 1990). Cempírek et al. (2010) measured 0.019-  
292 0.079 Li pfu in almandine from leucocratic granulite of Czech Republic. For synthetic Li-rich  
293 majoritic garnet, Yang et al. (2009) provide 1.96 Li pfu whereas up to about 7 Li atoms pfu were  
294 reported for other synthetic garnets (Wang and Lai 2012). This element occurs as a major chemical  
295 component in the garnet end member cryolithionite,  $\text{Na}_3\text{Al}_2\text{Li}_3\text{F}_{12}$  (Geller 1971).

296       Regarding the fluorine concentration, in our samples it ranges from 0.004(1) to 0.040(4)  
297 wt% (**Table 2**) which corresponds to 0.001-0.010 atoms per formula unit. Literature data indicate F  
298 content ranging from ~ 0.1 to 5 wt% in Ti-garnets with andradite and andradite-grossular  
299 component (Flohr and Ross 1989; Manning and Bird 1990; Barbanson and Bastos Neto 1992;  
300 Visser 1993; Ulrych et al. 1994; Armbruster et al. 1998; Freiburger et al. 2001; Faryad and Dianiška  
301 2003) and is equal to ~ 6 wt% in the F-rich hibschite (Chakhmouradian et al. 2008), showing that in  
302 our garnets all values are on the lower end of the natural variability interval.

303

#### 304 **Iron speciation**

305       The iron oxidation state was determined both via electron microprobe analysis – the Flank  
306 method (Höfer and Brey 2007) - and Mössbauer spectroscopy. Specifically, the Flank method was  
307 used on the same single crystals which underwent structure refinements, whereas Mössbauer  
308 analyses were carried out on powders of the W6 and W16 samples. The results are reported  
309 respectively in **Tables 2** and **3**. Mössbauer spectra of samples W6 and W16 are in **Figure 2a, 2b**,  
310 whereas comparison between Mössbauer and Flank method is in **Figure 3**. In **Table 3** Mössbauer  
311 data on W12, NZALA and ZER2 samples from previous work (Pedrazzi et al. 2002) are also  
312 reported for comparison. The fitting of the room temperature Mössbauer spectra **Figure 2** allowed  
313 to identify different iron species:  $^Y\text{Fe}^{3+}$ ,  $^Z\text{Fe}^{3+}$ ,  $^Z\text{Fe}^{2+}$ ,  $^Y\text{Fe}^{2+}$ . The assignment and the values of the  
314 hyperfine parameters (**Table 3**) are in agreement with the results of previous investigations on Ti-  
315 garnets (Ortalli et al. 1994; Pedrazzi et al. 1998, 2002; Scordari et al. 1999; Schingaro et al. 2004;

316 Dyar et al. 2012). In particular, the  ${}^Z\text{Fe}^{2+}$  species has been reported in other Mössbauer spectra on  
317 Ti-garnets (Kühberger et al. 1989; Locock et al. 1995; Chakhmouradian and McCammon 2005) but  
318 its interpretation is still uncertain and, recently, Chakhmouradian and McCammon (2005) have  
319 reinterpreted this component as  ${}^Y\text{Fe}^{2+} \leftrightarrow {}^Z\text{Fe}^{3+}$  electron transfer. However, attempts to fit the  
320 spectra of W6, W16 and NZALA samples according to the model 2 in Chakhmouradian and  
321 McCammon (2005) were unsuccessful.

322 The comparison between  $\text{Fe}^{3+}/\Sigma\text{Fe}$  as measured by Mössbauer and Flank method derived  
323 (**Figure 3**) indicates a good correlation ( $R^2 \sim 0.8$ ) between the two sets of measurements. The  
324 observed discrepancies, specifically for the W12 and W16 samples, may be due to the crystal  
325 chemical heterogeneity of the sample, so that the single crystals selected for EPMA and SCXRD  
326 may be not representative of the powders (see also the section XRPD below).

327

328

## 329 **Structural features**

### 330 ***XRPD results***

331 The X-ray powder diffraction analysis was performed on all the study samples (see the  
332 patterns in **Figure 4**) with the exception of ZER2, whose amount was too scarce to be measured.  
333 The qualitative analysis evidenced that no phase impurity occurs. However, splitting or asymmetry  
334 of the diffraction peaks is observed, suggesting the presence in our powders of different garnet  
335 phases with similar unit cell parameters (**Figure 5**). Indeed in all samples, at least two cubic garnet  
336 phases (labelled phase I and II on the basis of the relative abundances) were clearly distinguished  
337 and their weight fractions and cell parameters were refined using GSASII; the results are shown in  
338 **Table 4**. In the case of W6 and W16 samples, a third phase seems to be present (**Figure 5**) but the  
339 attempts to refine it was unsuccessful. These results are in agreement with recent findings relevant  
340 to the study of optical anomalies in garnets. In particular, these studies have shown that both Ti-  
341 bearing and Ti-free garnets can actually be a mixture of two or more cubic phases with slightly

342 different cell parameters and composition (Antao 2013, 2014; Antao and Klincker 2013; Antao and  
343 Round 2014). The consequent structural mismatch causes strain that results in low- to -strong  
344 degree of optical anisotropy (birefringence). In our case, the garnets appear not completely extinct  
345 upon observation under cross-polarized light, but did not show difference in chemical composition  
346 at least at the EPMA scale (see above). Similar results were reported for a Ti-andradite from  
347 Magnet Cove (Antao 2013). In brief, anomalous optical behavior is due to intergrowth of more than  
348 one cubic phase, that, if occurs at a fine scale, leads to homogeneous EPMA data, whereas at a large  
349 scale should be detected as a slight variation of chemical composition. To the best of our  
350 knowledge, it is the first time that a mixture of cubic phases has been detected for Ti-garnets with  
351 laboratory instrumentation. In addition, data in **Table 4** show that the dominant phase of the  
352 mixture (phase I) has, in most cases, unit cell parameters similar to those obtained from the relevant  
353 samples in SCXRD analysis (see below).

354

### 355 *SCXRD results*

356 The main results of SCXRD investigation, in particular about crystal data, data-collection  
357 parameters and figures of merit on structure refinements, are also summarised in **Table 4**. Refined  
358 site positions, atomic occupancies and anisotropic displacement parameters are listed in **Table 5**  
359 whereas distances and distortional parameters are reported in **Table 6**.

360 All structure refinements converged to good values of the discrepancy factors:  $1.65 \leq R_1 \leq$   
361  $2.09 \%$  and  $2.35 \leq wR_2 \leq 3.02 \%$ .

362 The cell-edges variation of the analysed crystals (**Table 4**) reflects different Ti contents  
363 (**Table 2**), a correlation already pointed out by Howie and Woolley (1968). In particular, a positive  
364 trend of the  $a$  parameter versus the  $\text{TiO}_2$  content has been found (**Figure 6**).

365 However, by inspection of **Figure 7** it is evident that the  $a$ -cell parameter increment depends  
366 on the increase of both the  $\langle X-O \rangle$  ( $R^2 = 0.90$  in **Figure 7a**) and  $Z-O$  ( $R^2 = 0.86$  in **Figure 7c**)

367 whereas the dependence from the Y-O variation seems to be negligible ( $R^2 = 0.004$  in **Figure 7b**).  
368 Since the X-site composition is almost constant in the study samples (see **Table 7**), the increase of  
369  $\langle X-O \rangle$  is induced by the polyhedral edge-sharing (X/Z) occurring in the garnet structure.

370 From **Table 6** it can be noticed that the  $\Delta(X-O)$  and  $\alpha$  values are in the range of variability  
371 for the known natural silicate garnets (Ungaretti et al. 1995; Yang et al. 2009). The tendency to the  
372 decrease of  $\Delta(X-O)$  with increasing  $Fe^{3+}$  content along the grossular-andradite join (Ungaretti et al.  
373 1995) is also present in our samples, where it appears also related to the  $Fe^{3+} + Ti$  content.

374 Octahedral and tetrahedral sites in garnets are variously distorted, as evident from the  
375 analysis of octahedral angle variance and tetrahedral angle variance (OAV and TAV, **Table 6**)  
376 which, respectively, quantifies the deviation from the ideal value of  $90^\circ$  and  $109.47^\circ$  of the relevant  
377 polyhedra (**Table 6, Figures 8 and 9**). In particular, the tetrahedron is the most distorted polyhedron  
378 in garnets and the distortion increases with increasing the  $Z(Fe^{2+}+Al+Fe^{3+}+Ti)$  content (**Figure 8**).  
379 On the other hand, since each tetrahedron in the garnet structure shares edges with two  
380 dodecahedra, the shared O-O tetrahedral edges,  $S(Z)$ , are always shorter than the unshared ones,  
381  $U(Z)$  and, at the same time, the tetrahedron is elongated along the  $\bar{4}$  axis (see  $t_{SZ}$ , the distance  
382 between shared edges in **Table 6**) for a better screening of the repulsive interaction between the X  
383 and Z cations. The octahedron is most distorted in grossular and becomes more regular with the  
384 entrance of high charge cations or of trivalent cations different from  $Al^{3+}$  (**Figure 9**). In addition,  
385 substitutions at Y affect the  $t_{SY}$  parameter in that, starting from pure grossular, where the octahedron  
386 is flattened along the  $\bar{3}$  axis, if a cation larger than Al occurs at Y the octahedron tends to elongate  
387 along the same axis, as also observed by other authors (Ungaretti et al. 1995).

388 The ZER2 sample has bond distances and distortion parameters very similar to that of pure  
389 andradite (Adamo et al. 2011). For instance, for this sample the  $\langle D-O \rangle$  parameter (2.131 Å) is  
390 identical to that of the pure andradite (2.132 Å, Adamo et al. 2011) and is a consequence of its short

391 Z-O distance (**Table 6**), indicating a low extent of substitution at the Z site. The increase in the Z-O  
392 distances in the other samples accounts for a greater extent of schorlomite and hydrogarnet  
393 substitutions. These features entail the increase of the  $\langle D-O \rangle$  parameters up to values close to that  
394 (2.186 Å) of kimzeyite of Schingaro et al. (2001), see **Table 6**.

395

### 396 **Crystal chemical formulae**

397 Grew et al. (2013) suggested a procedure to perform a cation distribution for Ti-garnets  
398 basing only on chemical data; the results obtained using their spreadsheet are reported in **Table 7**.  
399 In the same table we also reported the structural formulae of the study garnets, obtained using a  
400 multimethodic approach adopted in the present work. Specifically, they were calculated combining  
401 the EPMA-SIMS data with the Mössbauer results. The latter were considered representative of the  
402 single crystals. This assumption is generally sensible, on the basis of the Flank method analysis (see  
403 above). From the two sets of crystal chemical formulae, mean atomic numbers as well as bond  
404 distances using ionic radii from Shannon (1976) have been calculated. These values are shown in  
405 **Table 8** where they are compared with those derived from the structure refinement.

406 Samples W12 and ZER2 contain the smallest number of Fe species ( ${}^Y\text{Fe}^{3+}$ ,  ${}^Z\text{Fe}^{3+}$  the former  
407 and only  ${}^Y\text{Fe}^{3+}$  the latter, see **Table 3**) and in particular ZER2 has the simplest composition among  
408 the whole suite here considered. Comparison to the formulae derived through the approach devised  
409 by Grew et al. (2013) indicates that charge balance tends to overestimate the  ${}^Y\text{Fe}^{2+}$  specie. For  
410 example, for the ZER2 garnet, both the Flank method and Mössbauer analysis provide  $\text{Fe}^{3+}/\Sigma\text{Fe} =$   
411 100%, whereas from Grew et al. (2013)  $\text{Fe}^{3+}/\Sigma\text{Fe} = 86\%$  is estimated (see **Tables 2, 3, 7** and **Figure**  
412 **3**). Comparison to the crystallographic data (**Table 8**) shows that a better agreement is obtained  
413 with our multi-methodic approach for the Y site, that allows a better modeling of this site in terms  
414 of mean atomic number as well as bond distances. In particular good agreement is found between  
415 the Y-O distance derived from the X-ray refinement ( $Y-O_{X\text{-ref}}$ ) and that calculated from the EPMA

416 (Y-O<sub>EPMA\*</sub>) with  $\Delta = (Y-O_{X-ref}) - (Y-O_{EPMA*}) = 0.008 \text{ \AA}$  (see **Table 8**). On the contrary, if the  
417 approach in Grew et al. (2013) is used,  $\Delta$  increases to 0.021  $\text{\AA}$ . Note that the use of the directly  
418 measured iron speciation implies that the Y site hosts significant amount of Ti<sup>3+</sup>, as previously  
419 found in the Val Malenco Ti-bearing garnets (Müntener and Hermann, 1994; 175, 274, 275, 276  
420 crystals in Merli et al. 1995). As found for the sample ZER2, also in sample W12 <sup>Y</sup>Fe<sup>2+</sup> is  
421 overestimated, since Mössbauer spectrum only shows Fe<sup>3+</sup> species (**Tables 2, 3**) and our formula, as  
422 before, provides a better modeling of the octahedral site.

423 In the case of sample W6 the Mössbauer spectrum is more complex and in particular the  
424 <sup>Z</sup>Fe<sup>2+</sup> species has been detected. Although controversial (Chakhmouradian and McCammon 2005)  
425 this species is taken into account by Grew et al. (2013) in the procedure for site allocation of cations  
426 in Ti-garnets. However, the substitution explaining the <sup>Z</sup>Fe<sup>2+</sup> uptake in the garnet structure is not  
427 specified. In the literature two mechanisms have been proposed for the charge balance in this case:  
428 <sup>Z</sup>Si<sup>4+</sup> + 2O<sup>2-</sup> ↔ <sup>Z</sup>R<sup>2+</sup> + 2(OH)<sup>-</sup> (Kühberger et al. 1989) and 2<sup>Y</sup>Ti<sup>4+</sup> + <sup>Z</sup>Fe<sup>2+</sup> ↔ 2<sup>Y</sup>Fe<sup>3+</sup> + <sup>Z</sup>Si (Locock et  
429 al. 1995). Another mechanism <sup>Y</sup>U<sup>6+</sup> + <sup>Z</sup>Fe<sup>2+</sup> = <sup>Y</sup>U<sup>5+</sup> + <sup>Z</sup>Fe<sup>3+</sup> was proposed for elbrusite (Galuskina et  
430 al. 2010a). In our case, the mechanism of Kühberger et al. (1989) leads to major inconsistencies  
431 with SIMS data relevant to the hydrogen quantification. Accordingly, the mechanism proposed by  
432 Locock et al. (1995) was adopted.

433 For sample NZALA, that contains negligible <sup>Z</sup>Fe<sup>2+</sup>, our distribution and the one from Grew  
434 et al. (2013) are almost identical. Notice that the calculated and measured Fe<sup>3+</sup>/ΣFe values are very  
435 similar (see **Tables 2, 3**). Although a general good agreement with X-ray data is observed for both  
436 formulae, the difference between Y-O<sub>EPMA</sub> and Y-O<sub>X-ref</sub> distances gives < 0.01  $\text{\AA}$  in our case and ~  
437 0.02  $\text{\AA}$  considering only chemical data (see **Table 8**).

438 For sample W16, Mössbauer and charge balance derived Fe<sup>3+</sup>/ΣFe coincide, whereas a  
439 discrepancy is observed with respect to the value determined via the Flank method (see **Tables 2, 3**  
440 and **Figure 3**). The difference between cell parameter from single crystal and powder is  $\Delta a \sim 0.01-$

441 0.02 Å. The above evidences indicate that the single crystal is not representative of the powder.  
442 Several cation distributions have been checked, until the best fit to the data from different  
443 techniques was obtained by considering  $\text{Fe}^{3+}/\Sigma\text{Fe}$  from Flank method and the iron site population  
444 from Mössbauer.

445 Sample W6 has ferrous iron only at tetrahedral site. As in previous sample, inspection of  
446 **Table 4** evidences that the single crystal has cell parameter shorter than those found in the powder  
447 ( $\Delta a \sim 0.01\text{-}0.02$  Å). Accordingly, for the study single crystal a lower degree of tetrahedral  
448 substitution is expected with respect to the analysed powder. The best fit to all the experimental  
449 data is obtained varying the  $^Z\text{Fe}^{2+}$  component within one standard deviation.

450 The main substitution mechanisms affecting the studied garnets are:

451 1)  $^{\text{VI}}\text{R}^{4+} + ^{\text{IV}}\text{R}^{3+} \leftrightarrow ^{\text{IV}}\text{Si} + ^{\text{VI}}\text{R}^{3+}$  (schorlomite substitution);

452 2)  $^{\text{Y}}\text{R}^{2+} + ^{\text{Z}}\text{R}^{4+} \leftrightarrow 2^{\text{Y}}\text{R}^{3+}$  (morimotoite substitution);

453 3)  $^{\text{Y}}\text{R}^{3+} \leftrightarrow ^{\text{Y}}\text{Fe}^{3+}$  (andradite substitution);

454 where  $^{\text{Y}}\text{R}^{2+} = \text{Fe}^{2+}, \text{Mg}^{2+}, \text{Mn}^{2+}$ ;  $^{\text{Z}}\text{R}^{4+} = \text{Ti}$ ;  $^{\text{Y}}\text{R}^{3+} = \text{Fe}^{3+}, \text{Al}^{3+}, \text{Cr}^{3+}$ ;  $^{\text{Z}}\text{R}^{3+} = \text{Fe}^{3+}, \text{Al}^{3+}$ .

455 Minor substitutions, such as:

456 a)  $2^{\text{Y}}\text{Ti}^{4+} + ^{\text{Z}}\text{Fe}^{2+} \leftrightarrow 2^{\text{Y}}\text{Fe}^{3+} + ^{\text{Z}}\text{Si}$ ;

457 b)  $(\text{SiO}_4)^{4-} \leftrightarrow (\text{O}_4\text{H}_4)^{4-}$ ;

458 c)  $\text{F}^- \leftrightarrow \text{OH}^-$ ;

459 d)  $^{\text{Y}}\text{R}^{4+} + ^{\text{X}}\text{R}^+ \leftrightarrow ^{\text{Y}}\text{R}^{3+} + ^{\text{X}}\text{Ca}^{2+}$ , with  $^{\text{Y}}\text{R}^{4+} = \text{Ti}, \text{Zr}$ ;  $^{\text{Y}}\text{R}^{3+} = \text{Fe}^{3+}, \text{Al}, \text{Cr}^{3+}$ ;  $^{\text{X}}\text{R}^+ = \text{Na}, \text{Li}$  also occur.

460 On the whole, light elements, although occurring in detectable amounts, do not play a significant  
461 crystal chemical role. No systematic trend was here evidenced from the analysis of Ti and water  
462 content in relation to the garnets host rocks (see also **Figure 1**).

463 For a better crystal chemical comparison, in **Table 7**, in addition to the structural formulae  
464 derived for the samples under study, also formulae taken from the literature are reported, selected in  
465 order to include natural end-member garnets (grossular, Novak and Gibbs 1971; andradite, Adamo

466 et al. 2011) as well as Z-substituted Ti garnets for which cation partition was provided on the basis  
467 of evidences from multiple methods-combination of chemical and/or X-ray diffraction and/or  
468 spectroscopic data (Müntener and Hermann 1994; Ulrych et al. 1994; Locock et al. 1995; Scordari  
469 et al. 1999; Schingaro et al. 2001; Chakhmouradian and McCammon 2005; Katerinopoulou et al.  
470 2009; Antao 2013, 2014). It can be seen that the chemical complexity of Ti-garnets is such that  
471 every sample has to be considered on a one to one basis. In some cases, in order to get the best  
472 agreement, with X-ray data, Ti has to be distributed over octahedral and tetrahedral site (sample W6  
473 and W16, this work; Scordari et al. 1999; Katerinopoulou et al. 2009). Evidences of the occurrence  
474 of Ti at Z site have been reported by Malitesta et al. (1995) and Armbruster et al. (1998) for garnets  
475 with similar composition, as well as in Si-poor natural garnets, like elbrusite and bitikleite  
476 (Galuskina et al. 2010a, 2010b). The Ti valence state is a controversial topic in the Ti-garnets  
477 literature and has been thoroughly reviewed by Grew et al. (2013). In particular, in natural Ti-  
478 garnets, Malitesta et al.(1995) found significant  $Ti^{3+}$  using X-ray Photoelectron Spectroscopy  
479 (XPS), whereas Waychunas (1987) and Locock et al. (1995) detected low or negligible  $Ti^{3+}$  via X-  
480 ray Absorption Near Edge Structure (XANES) spectroscopy. This discrepancy may be due to a  
481 greater contribution of the mineral surface in the case of XPS (Grew et al. 2013) as well as to the  
482 problems in the interpretation of XPS signals related to the adopted method of background  
483 removing (Guascito et al. 2014). In the present work, the Ti speciation has not been determined by  
484 direct measurements, but it was constrained indirectly through the quantification of the water  
485 content, the determination of the iron oxidation state and the balance of the substitution mechanisms  
486 in garnets.

487         The two approaches discussed above and used to calculate the crystal chemical formulae  
488 lead to a different classification of the study samples as shown in the plot of **Figure 10**. In  
489 particular, when the only chemical data are used, the samples fall in the schorlomite field together  
490 with the Afrikanda schorlomite (Chakhmouradian and McCammon 2005) and the morimotoite

491 (Antao 2014). On the contrary, when the multimethodic approach is used, the study garnets plot in  
492 the andradite field very close to most of the considered literature garnets (Müntener and Hermann  
493 1994; Ulrych et al. 1994; Locock et al. 1995; Amthauer and Rossman 1998; Katerinopoulou et al.  
494 2009; Phichaikamjornwut et al. 2011; Antao 2013). Notice that kimzeyite sample investigated by  
495 Schingaro et al. (2001) should be classified as belonging to the garnet group rather than to  
496 schorlomite group. Generally speaking, the approach to the garnet crystal chemical formula  
497 proposed by Grew et al. (2013) is effective and constitutes a good starting point in absence of other  
498 information, but then the obtained formula needs to be refined by comparison at least to X-ray data  
499 and possibly also to element specific techniques selected depending on the peculiar composition of  
500 the sample. Major chemical variability is, indeed, observed for the Y site, that is why a totally  
501 chemical approach is here found to have problems with the modeling cation distribution at the Y  
502 site.

503

504

## IMPLICATIONS

505 Garnet is a widespread mineral stable in wide range of temperature (from < 300 to 2000°C)  
506 and pressure (from ambient pressure to 25 GPa). The renewed interest in the garnet species is  
507 testified by a recent issue of Elements (Volume 9(6), December 2013) devoted to the garnet  
508 supergroup of minerals. The relevance of elemental substitutions in determining the properties of  
509 garnets has been highlighted in Grew et al. (2013), Geiger (2013) and Antao (2013). In particular,  
510 Grew et al. (2013) evidence that recently (2009-2010) 10 new garnet species with unusual  
511 constituents were approved by the Commission on New Minerals, Nomenclature and Classification  
512 of the International Mineralogical Association and the 32 approved species also encompass three  
513 ungrouped species but new species are expected due to the extreme compositional variations in  
514 natural garnets. Geiger (2013), other than reviewing synthetic non silicate garnets and the relevant  
515 technological employment, stresses the significance of studying substitutional solid solutions in

516 natural garnets. Cation substitutions involve strain fields resulting in structural heterogeneities from  
517 the scale of the unit cell to the nanoscale. Structural and chemical bonding properties of garnets are  
518 believed to control element partitioning (Wood et al. 2013) and thermodynamic behavior of the  
519 garnet solid solutions. For a complete characterization of these phases, both techniques sensitive to  
520 long-range ordering (such as X-ray diffraction) and to short range ordering (spectroscopic  
521 techniques) are needed. This is the approach adopted in the present work. Regarding natural Ti-  
522 garnets, their relevance from a petrological point of view has been mentioned in the introduction  
523 section. However, it is generally recognized that determination of cation site population is really  
524 complicated for such compositions. In turn cation exchange mechanisms produce polyhedral  
525 distortions, that have been reported here, but unravelling the contribution of each of the multiple  
526 substitutions requires further work. In this study, the detailed characterization of substitution  
527 mechanisms by single crystal X-ray diffraction is associated to the observation of occurrence of  
528 multiple cubic phases from laboratory XRPD data. Even if, in our case, the samples appeared  
529 homogeneous at the EPMA scale it is here suggested that compositional differences at the nanoscale  
530 may occur, as found by other authors (Antao 2013). These findings, in turn, may have implication  
531 for the study of garnets zonation (see, for instance, Matthews et al. 1992; Gwalani et al. 2000;  
532 Agrosi et al., 2002, 2011). Complex zoning occurring in primary Ti-garnets and involving variation  
533 of Ca, Ti, Zr and Al was described by Gwalani et al. (2000). These authors were able to correlate it  
534 to the multiple events that occurred during the magma crystallization, depicting a multi-step  
535 magmatic history from fractional crystallization, to magma mixing to closed system crystallization,  
536 to fluctuation of P-T,  $f_{O_2}$  conditions. Agrosi et al. (2002) studied the sector zoning in Ti-andradite  
537 from Colli Albani and found that morimotoite substitution was present in {110} sectors whereas  
538 both morimotoite and schorlomite substitutions affected {121} sectors. The strain associated to the  
539 presence of the schorlomite substitution in {121} sectors could be correlated to the higher growth  
540 rate of these sectors with respect to the others by the layer-by layer mechanism. Subsequently, for

541 the same Ti-garnets from Colli Albani concentric zoning was also observed, that, together with the  
542 identification of growth marks, allowed to characterize the growth environment (Agrosi et al. 2011).  
543 Very recently (Antao et al. 2015) correlated the occurrence of multiple cubic phases in Ti-rich  
544 andradite to optical anomalies (birefringence) and to oscillatory zoning related to andradite-rich and  
545 andradite poor cubic phases or to subtle chemical variations involving Ti, Fe, Al and Mg atoms  
546 concentrations. All the above considerations indicate the high sensitivity of the Ti-garnet structure  
547 in that even slight element abundance variation has detectable effect on the crystal structure (in  
548 terms of cell edges, bond distances, etc.) as well as the potential use of the garnet crystal chemistry  
549 at the micrometric or even nanometric scale to derive geological inferences (i.e. magma evolution,  
550 thermal history, growth environment, late stage reactions, etc.).

551

552

## ACKNOWLEDGMENTS

553 The authors are grateful to Prof. Stefano Poli (University of Milano) for the facilities at the  
554 Electron Microprobe Laboratory and Dr. Nadia Malaspina for the assistance during the ‘Flank  
555 method’ analyses at the Dipartimento di Scienze della Terra, University of Milano. Prof. Thomas  
556 Armbruster is gratefully thanked for providing NZALA and ZER2 garnet samples. Thanks are due  
557 to the Associate Editor, Gatta Giacomo Diego, and to Redhammer Günther Josef and a anonymous  
558 Referee that contributed to significantly improve the manuscript.

559 The XRPD laboratory at the Dipartimento di Scienze della Terra and Geoambientali,  
560 University of Bari “Aldo Moro”, was funded by Potenziamento Strutturale PONA3\_00369  
561 “Laboratorio per lo Sviluppo Integrato delle Scienze e delle TECnologie dei Materiali Avanzati e  
562 per dispositivi innovativi (SISTEMA)”.

563 This work was also supported by the COFIN-MIUR.

564

565

## REFERENCES

- 566 Adamo, I., Gatta, G.D., Rotiroti, N., Diella, V., and Pavese, A. (2011) Green andradite stones:  
567 gemmological and mineralogical characterisation. *European Journal of Mineralogy*, 23, 91-100.
- 568 Agrosi, G., Schingaro, E., Pedrazzi, G., Scandale, E., and Scordari, F. (2002) A crystal chemical  
569 insight into sector zoning of a titanian andradite ('melanite') crystal. *European Journal of*  
570 *Mineralogy*, 14(1), 785-794.
- 571 Agrosi, G., Scandale, E., and Tempesta, G. (2011) Growth marks of titanian-andradite crystals from  
572 Colli Albani (Italy). *Periodico di Mineralogia*, 80(1), 89-104.
- 573 Amthauer, G. and Rossman, G.R. (1998) The hydrous component in andradite garnet. *American*  
574 *Mineralogist*, 83, 835-840.
- 575 Antao, S.M. (2013) The mystery of birefringent garnet: is the symmetry lower than cubic?. *Powder*  
576 *diffraction*, 28(4), 281-288.
- 577 Antao, S.M. (2014) Crystal structure of morimotoite from Ice River, Canada. *Powder diffraction*,  
578 29(4), 325-330.
- 579 Antao, S.M. and Klincker, A.M. (2013) Origin of birefringence in andradite from Arizona,  
580 Madagascar, and Iran. *Physics and Chemistry of Minerals*, 40, 575-586.
- 581 Antao, S.M. and Round, S.A. (2014) Crystal chemistry of birefringent spessartine. *Powder*  
582 *diffraction*, 29(3), 233-240.
- 583 Antao, S.M., Mohib, S., Zaman, M., and Marr, R.A. (2015) Ti-rich andradites: chemistry, structure,  
584 multi-phases, optical anisotropy, and oscillatory zoning. *Canadian Mineralogist*, DOI:  
585 10.3749/canmin.1400042.
- 586 Armbruster, T. (1995) Structure refinement of hydrous andradite,  $\text{Ca}_3\text{Fe}_{1.54}\text{Mn}_{0.20}$   
587  $\text{Al}_{0.26}(\text{SiO}_4)_{1.65}(\text{O}_4\text{H}_4)_{1.35}$ , from the Wessels mine, Kalahari manganese field, South Africa.  
588 *European Journal of Mineralogy*, 7, 1221-1225.
- 589 Armbruster, T., Birrer, J., Libowitzky, E., and Beran, A. (1998) Crystal chemistry of Ti-bearing  
590 andradites. *European Journal of Mineralogy*, 10, 907-921.

- 591 Balic Zunic, T. and Vickovic, I. (1996) IVTON- a program for the calculation of geometrical  
592 aspects of crystal structures and some crystal chemical applications. Journal of Applied  
593 Crystallography, 29, 305-306.
- 594 Barbanson, L. and Bastos Neto, A.C. (1992) Hydroandradite titanifère fluorée et grenat  
595 ( $\text{Spe}_{39}\text{Gro}_{31}\text{Alm}_{23}\text{And}_6$ ) fluoré des granitoïdes du district à fluorine de Santa Catarina  
596 (Brésil): description minéralogique, mécanisme d'incorporation du fluor, signification  
597 pétrologique et métallogénique. Comptes Rendus de l'Académie des Sciences, Série II, 314,  
598 63-69.
- 599 Basso, R. and Cabella, R. (1990) Crystal chemical study of garnets from metarodingites in the  
600 Voltri Group metaophiolites (Ligurian Alps, Italy). Neues Jahrbuch für Mineralogie  
601 Monatshefte, 1990, 127-136.
- 602 Basso, R., Cimmino, F., and Messiga, B. (1984a) Crystal chemistry of hydrogarnets from three  
603 different microstructural sites of a basaltic metarodingite from the Voltri Massif (Western  
604 Liguria, Italy). Neues Jahrbuch für Mineralogie Abhandlungen, 148, 246-258.
- 605 Basso, R., Cimmino, F., and Messiga, B. (1984b) Crystal chemical and petrological study of  
606 hydrogarnets from a Fe-gabbro metarodingite (Gruppo di Voltri, Western Liguria, Italy). Neues  
607 Jahrbuch für Mineralogie Abhandlungen, 150, 247-258.
- 608 Bell, D.R., Rossman, G.R., and Moore, R.O. (2004) Abundance and partitioning of OH in a high-  
609 pressure magmatic system: megacrysts from the Monastery kimberlite, South Africa. Journal of  
610 Petrology, 45(8), 1539-1564.
- 611 Betteridge, P.W., Carruthers, J.R., Cooper, R.I., Prout, K., and Watkin, D.J. (2003) Crystals version  
612 12: software for guided crystal structure analysis. Journal of Applied Crystallography, 36, 1487.
- 613 Born, L. and Zemann, J. (1964) Abstandsberechnungen und gitterenergetische Berechnungen an  
614 Granaten. Contributions to Mineralogy and Petrology, 10, 2-23.

- 615 Brod, J.A., Junqueira-Brod, T.C., Gaspar, J.C., Gibson, S.A., and Thompson, R.N. (2003) Ti-rich  
616 and Ti-poor garnet from the Tapira carbonatite complex, SE Brazil: fingerprinting fractional  
617 crystallization and liquid immiscibility. In 8<sup>th</sup> International Kimberlite Conference, Extended  
618 Abstracts (CD), FLA\_0399.pdf, p. 5.
- 619 Bruker (2003a) COSMO (Version 1.61), Bruker AXS Inc., Madison, Wisconsin, USA.
- 620 Bruker (2003b) SAINT (Version 7.60A). Bruker AXS Inc., Madison, Wisconsin, USA.
- 621 Cempírek, J., Novák, M., Dolníček, Z., Kotková, J., and Škoda, R. (2010) Crystal chemistry and  
622 origin of grandierite, omineite, boralsilite, and werdingite from the Bory Granulite Massif,  
623 Czech Republic. *American Mineralogist*, 95, 1533-1547.
- 624 Chakhmouradian, A.R. and McCammon, C.A. (2005) Schorlomite: a discussion of the crystal  
625 chemistry, formula, and inter-species boundaries. *Physics and Chemistry of Minerals*, 32, 277-  
626 289.
- 627 Chakhmouradian, A.R., Cooper, M.A., Medici, L., Hawthorne, F.C., and Adar, F. (2008) Fluorine-  
628 rich hibschite from silicocarbonatite, Afrikanda complex, Russia: crystal chemistry and  
629 conditions of crystallization. *Canadian Mineralogist*, 46, 1033-1042.
- 630 Cussen, E.J. (2006) The structure of lithium garnets: cation disorder and clustering in a new family  
631 of fast Li<sup>+</sup> conductors. *Chemical Communications*, 4, 412-413.
- 632 Deer, W.A., Howie, R.A., and Zussman, J. (1982) *Rock-forming minerals, Orthosilicates*, 1A,  
633 Longman, New York.
- 634 Dingwell, D.B. and Brearley, M. (1985) Mineral chemistry of igneous melanite garnets from  
635 analcite-bearing volcanic rocks, Alberta, Canada. *Contributions to Mineralogy and Petrology*,  
636 90, 29-35.
- 637 Dwarzski, R.E., Draper, D.S., Shearer, C.K., and Agee, C.B. (2006). Experimental insights on  
638 crystal chemistry of high-Ti garnets from garnet-melt partitioning of rare-earth and high-field-  
639 strength elements. *American Mineralogist*, 91(1), 1536-1546.

- 640 Dyar, M.D., Schaefer, M.W., Sklute, E.C., and Bishop, J.L. (2008): Mössbauer spectroscopy of  
641 phyllosilicates: effect of fitting models on recoil-free fractions and redox ratios. *Clay Minerals*,  
642 43, 3-33.
- 643 Dyar, M.D., Breves, E.A., Emerson, E., Bell, S.W., Nelms, M., Ozanne, M.V., Pell, S.E.,  
644 Carmosino, M.L., Tucker, J.M., Gunter, M.E., Delaney, J.S., Lanzirotti, A., and Woodland, A.B.  
645 (2012) Accurate determination of ferric iron in garnets by bulk Mössbauer spectroscopy and  
646 synchrotron micro-XANES. *American Mineralogist*, 97(10), 1726-1740.
- 647 Eeckhout, S.G., Castañeda, C., Ferreira, A.C.M., Sabioni, A.C.S., de Grave, E., and Vasconcelos,  
648 D.C.L. (2002) Spectroscopic studies of spessartine from Brazilian pegmatites. *American*  
649 *Mineralogist*, 87, 1297-1306.
- 650 Faryad, S.W. and Dianiška, I. (2003) Ti-bearing andradite-prehnite-epidote assemblage from the  
651 Malá Fatra granodiorite and tonalite (Western Carpathians). *Schweizerische Mineralogische und*  
652 *Petrographische Mitteilungen*, 83, 47-56.
- 653 Ferro, O., Galli, E., Papp, G., Quartieri, S., Szakáll, S., and Vezzalini, G. (2003) A new occurrence  
654 of katoite and re-examination of the hydrogrossular group. *European Journal of Mineralogy*, 15,  
655 419-426.
- 656 Flohr, M.J.K. and Ross, M. (1989) Alkaline igneous rocks of Magnet Cove, Arkansas:  
657 Metasomatized ijolite xenoliths from Diamond Jo quarry. *American Mineralogist*, 74, 113-131.
- 658 Freiburger, R., Hecht, L., Cuney, M., and Morteani, G. (2001) Secondary Ca-Al silicates in plutonic  
659 rocks: implications for their cooling history. *Contribution to Mineralogy and Petrology*, 141,  
660 415-429.
- 661 Galuskin, E.V. (2005) Minerals of the vesuvianite group from the achtarandite rocks (Wiluy River,  
662 Yakutia), 191 p. University of Silesia Publishing House, Katowice, Poland (in Polish).
- 663 Galuskina, I.O., Galuskin, E.V., Armbruster, T., Lazic, B., Kusz, J., Dzierżanowski, P., Gazeev,  
664 V.M., Pertsev, N.N., Prusik, K., Zadov, A.E., Winiarski, A., Wrzalik, R., and Gurbanov, A.G.

- 665 (2010a) Elbrusite-(Zr) - A new uranian garnet from the Upper Chegem caldera, Kabardino-  
666 Balkaria, Northern Caucasus, Russia. American Mineralogist, 95, 1172-1181.
- 667 Galuskina, I.O., Galuskin, E.V., Armbruster, T., Lazic, B., Dzierżanowski, P., Gazeev, V.M.,  
668 Prusik, K., Pertsev, N.N., Winiarski, A., Zadov, A.E., Wrzalik, R., and Gurbanov, A.G. (2010b)  
669 Bitikleite-(SnAl) and bitikleite-(ZrFe): New garnets from xenoliths of the Upper Chegem  
670 volcanic structure, Kabardino-Balkaria, Northern Caucasus, Russia. American Mineralogist, 95,  
671 959-967.
- 672 Geiger, C.A. (2013) Garnet: a key phase in nature, the laboratory and technology. Elements, 9(6),  
673 447-452.
- 674 Geller, S. (1971) Refinement of the crystal structure of cryolithionite,  $\{Na_3\}[Al_2](Li_3)F_{12}$ . American  
675 Mineralogist, 56, 18-23.
- 676 Grew, E.S., Chernosky, J.V., Werding, G., Abraham, K., Marquez, N., and Hinthorne, J.R. (1990)  
677 Chemistry of kornerupine and associated minerals, a wet chemical, ion microprobe, and X-ray  
678 study emphasizing Li, Be, B and F contents. Journal of Petrology, 31(5), 1025-1070.
- 679 Grew, E.S., Locock, A.J., Mills, S.J., Galuskina, I.O., Galuskin, E.V., and Hålenius, U. (2013)  
680 Nomenclature of the Garnet Supergroup. American Mineralogist, 98, 785-811.
- 681 Guascito, M.R., Mesto, E., Malitesta, C., Picca, R.A. and Scordari, F. (2014) The effect of XPS  
682 background removing method on the appraisal of Ti and Fe: The case of phlogopites and  
683 brookite. American Mineralogist, 99(1), 139-148.
- 684 Gwalani, L.G., Rock, N.M.S., Ramasamy, R., Griffin, B.J., and Mulai, B.P. (2000) Complexly  
685 zoned Ti-rich melanite-schorlomite garnets from Ambadungar carbonatite-alkalic complex,  
686 Deccan Igneous Province, Gujarat State, Western India. Journal of Asian Earth Sciences, 18,  
687 163-176.

- 688 Howie, R.A. and Woolley, A.R. (1968) The role of titanium and the effect of TiO<sub>2</sub> on the cell-size,  
689 refractive index, and specific gravity in the andradite-melanite-schorlomite series. Mineralogical  
690 Magazine, 36, 775-790.
- 691 Höfer, H.E. and Brey, G.P. (2007) The iron oxidation state of garnet by electron microprobe: Its  
692 determination with the flank method combined with major-element analysis. American  
693 Mineralogist, 92, 873-885.
- 694 Huggins, F.E., Virgo, D., and Huckenholz, H.G. (1977a) Titanium-containing silicate garnets. I.  
695 The distribution of Al, Fe<sup>3+</sup>, and Ti<sup>4+</sup> between octahedral and tetrahedral sites. American  
696 Mineralogist, 62, 475-490.
- 697 Huggins, F.E., Virgo, D., and Huckenholz, H.G. (1977b) Titanium-containing silicate garnets. II.  
698 The crystal chemistry of melanites and schorlmites. American Mineralogist, 62, 646-655.
- 699 Kalinichenko, A.M., Proshko, V.Ya., Matiash, I.V., Pavlishin, V.I., and Garmanik, M.Ya. (1987)  
700 NMR data on crystallochemical features of hydrogrossular. Geochemistry International, 24(4),  
701 132-135 (translated from Geokhimiya, 9, 1363-1366, 1986).
- 702 Katerinopoulou, A., Katerinopoulos, A., Voudouris, P., Bieniok, A., Musso, M., and Amthauer, G.  
703 (2009) A multi-analytical study of the crystal structure of unusual Ti-Zr-Cr-rich Andradite from  
704 the Maronia skarn, Rhodope massif, western Thrace, Greece. Mineralogy and Petrology, 95,  
705 113-124.
- 706 Koga, K., Hauri, E., Hirschmann, M., Bell, D. (2003) Hydrogen concentration analyses using SIMS  
707 and FTIR: Comparison and calibration for nominally anhydrous minerals. Geochemistry  
708 Geophysics Geosystems, 4(2), 1-20.
- 709 Kühberger, A., Fehr, T., Huckenholz, H.G., and Amthauer, G. (1989) Crystal chemistry of a natural  
710 schorlomite and Ti-andradites synthesized at different oxygen fugacities. Physics and Chemistry  
711 of Minerals, 16, 734-740.

- 712 Lagarec, K. and Rancourt, D.G. (1997) Extended Voigt-based analytic lineshape method for  
713 determining  $N$ -dimensional correlated hyperfine parameter distributions in Mössbauer  
714 spectroscopy. Nuclear Instruments and Methods in Physics Research B, 129, 266-280.
- 715 Lagarec, K. and Rancourt, D.G. (1998) RECOIL, Mössbauer Spectral Analysis Software for  
716 Windows (version 1.0). Department of Physics, University of Ottawa, Canada.
- 717 Lager, G.A., Armbruster, T., and Faber, J. (1987) Neutron and X-ray diffraction study of  
718 hydrogarnet  $\text{Ca}_3\text{Al}_2(\text{O}_4\text{H}_4)_3$ . American Mineralogist, 72, 756-765.
- 719 Lager, G.A., Armbruster, T., Rotella, F.J., and Rossman, G.R. (1989) OH substitution in garnets: X-  
720 ray and neutron diffraction, infrared, and geometric-modeling studies. American  
721 Mineralogist, 74, 840-851.
- 722 Locock, A., Luth, R.W., Cavell, R.G., Smith, D.G.W., and Duke, M.J.M. (1995) Spectroscopy of  
723 the cation distribution in the schorlomite species of garnet. American Mineralogist, 80, 27-38.
- 724 Lupini, L., Williams, C.T., and Wooley, A.R. (1992) Zr-rich garnet and Zr- and Th-rich perovskite  
725 from the Polino carbonatite, Italy. Mineralogical Magazine, 56, 581-586.
- 726 Malaspina, N., Poli, S., and Fumagalli, P. (2009) The oxidation state of metasomatized mantle  
727 wedge: insights from C–O–H-bearing garnet peridotite. Journal of Petrology, 50, 1533-1552.
- 728 Malaspina, N., Langenhorst, F., Fumagalli, P., Tumiati, S., and Poli, S. (2012)  $\text{Fe}^{3+}$  distribution  
729 between garnet and pyroxenes in mantle wedge carbonate-bearing garnet peridotites (Sulu,  
730 China) and implications for their oxidation state. Lithos, 146-147, 11-17.
- 731 Maldener, J., Hösch, A., Langer, K., and Rauch, F. (2003) Hydrogen in some natural garnets  
732 studied by nuclear reaction analysis and vibrational spectroscopy. Physics and Chemistry of  
733 Minerals, 30, 337-344.
- 734 Malitesta, C., Losito, I., Scordari, F., and Schingaro, E. (1995) XPS investigation of titanium in  
735 melanites from Monte Vulture (Italy). European Journal of Mineralogy, 7, 847-858.

- 736 Manning, C.E. and Bird, D.K. (1990) Fluorian garnets from the host rocks of the Skaergaard  
737 intrusion: implications for metamorphic fluid composition. *American Mineralogist*, 75, 859-873.
- 738 Matthews, M., Harte, B., and Prior, D. (1992) Mantle garnets: A cracking yarn. *Geochimica et*  
739 *Cosmochimica Acta*, 56(7), 2633-2642.
- 740 Merli, M., Callegari, A., Cannillo, E., Caucia, F., Leona, M., Oberti, R., and Ungaretti, L. (1995)  
741 Crystal-chemical complexity in natural garnets: structural constraints on chemical variability.  
742 *European Journal of Mineralogy*, 7, 1239-1249.
- 743 Müntener, O. and Hermann, J. (1994) Titanian andradite in a metapyroxenite layer from the  
744 Malenco ultramafics (Italy): implications for Ti-mobility and low oxygen fugacity. *Contribution*  
745 *to Mineralogy and Petrology*, 116, 156-168.
- 746 Novak, G.A. and Gibbs, G.V. (1971) The crystal chemistry of the silicate garnets. *American*  
747 *Mineralogist*, 56, 791-825.
- 748 Onuki, H., Akasaka, M., Yoshida, T., and Nedachia, M. (1982) Ti-Rich Hydroandradites from the  
749 Sanbagawa Metamorphic Rocks of the Shibukawa Area, Central Japan. *Contribution to*  
750 *Mineralogy and Petrology*, 80, 183-188.
- 751 Ortalli, I., Pedrazzi, G., Schingaro, E., and Scordari, F. (1994) Iron site populations from Mössbauer  
752 spectroscopy in Ti-bearing garnets from Mt. Vulture (Italy). *Hyperfine Interactions*, 91, 727-732.
- 753 Ottolini, L. and Hawthorne, F.C. (2001) SIMS ionization of hydrogen in silicates: a case study of  
754 kornerupine. *Journal of Analytical Spectrometry*, 16, 1266-1270.
- 755 Ottolini, L., Bottazzi, P., Zanetti, A., and Vannucci, R. (1995) Determination of Hydrogen in  
756 Silicates by Secondary Ion Mass Spectrometry. *The Analyst*, 120, 1309-1313.
- 757 Ottolini, L., Camara, F., Hawthorne, F.C., and Stirling, J. (2002) SIMS matrix effects in the analysis  
758 of light elements in silicate minerals: Comparison with SREF and EMPA data. *American*  
759 *Mineralogist*, 87, 1477-1485.

- 760 Pedrazzi, G., Schingaro, E., and Scordari, F. (1998) X-ray single crystal and Mössbauer study on  
761 Ti-garnets from the Tapira alkaline-carbonatite complex, Brazil. In E.B. Saitovitch, H.  
762 Rechenberg, and R.B. Scorzelli, Eds., *Hyperfine Interactions (C)*, 3, 321-324.
- 763 Pedrazzi, G., Schingaro, E., and Scordari, F. (2002) Mössbauer investigation on Ti-garnets from  
764 different geological environments. In M.F. Thomas, J.M. Williams, and T.C. Gibb, Eds.,  
765 *Hyperfine Interactions (C)*, 5, 457-460.
- 766 Phichaikamjornwut, B., Skogby, H., Ounchanum, P., Limtrakun, P., and Boonsoong, A. (2011)  
767 Hydrous components of grossular-andradite garnets from Thailand: thermal stability and  
768 exchange kinetics. *European Journal of Mineralogy*, 24, 107-121.
- 769 Platt, R.G. and Mitchell, R.H. (1979) The Marathon Dikes. I: Zirconium-rich titanian garnets and  
770 manganoan magnesian ulvöspinel-magnetite spinels. *American Mineralogist*, 64, 546-550.
- 771 Robinson, K., Gibbs, G.V., and Ribbe, P.H. (1971) Quadratic Elongation: A Quantitative Measure  
772 of Distortion in Coordination Polyhedra. *Science*, 172, 567-570.
- 773 Rossman, G.R. and Aines, R.D. (1991) The hydrous components in garnets: Grossular-  
774 hydrogrossular. *American Mineralogist*, 76, 1153-1164.
- 775 Saha, A., Ray, J., Ganguly, S., and Chatterjee, N. (2011) Occurrence of melanite garnet in syenite  
776 and ijolite-melteigite rocks of Samchampi-Samteran alkaline complex, Mikir Hills, Northeastern  
777 India. *Current Science*, 101(1), 95-100.
- 778 Schingaro, E., Scordari, F., Capitanio, F., Parodi, G., Smith, D., and Mottana, A. (2001) Crystal  
779 chemistry of kimzeyte from Anguillara, Mts. Sabatini, Italy. *European Journal of Mineralogy*,  
780 13, 749-759.
- 781 Schingaro, E., Scordari, F., Pedrazzi, G., and Malitesta, C. (2004) Ti and Fe speciation by X-ray  
782 Photoelectron Spectroscopy (XPS) and Mössbauer Spectroscopy for a full crystal chemical  
783 characterisation of Ti-garnets from Colli Albani (Italy). *Annali di chimica*, 94, 185-196.

- 784 Scordari, F., Schingaro, E., and Pedrazzi, G. (1999) Crystal chemistry of melanite from Mt. Vulture  
785 (Southern Italy). *European Journal of Mineralogy*, 11, 855-869.
- 786 Scordari, F., Dyar, M.D., Schingaro, E., Lacalamita, M., and Ottolini, L. (2010) XRD, micro-  
787 XANES, EMPA, and SIMS investigation on phlogopite single crystals from Mt. Vulture (Italy).  
788 *American Mineralogist*, 95, 1657-1670.
- 789 Shannon, R.D. (1976) Revised effective ionic radii and systematic studies of interatomic distances  
790 in halides and chalcogenides. *Acta Crystallographica*, A32, 751-767.
- 791 Sheldrick, G.M. (2003) SADABS, Program for Empirical Absorption Correction of Area Detector  
792 Data. University of Göttingen, Germany.
- 793 Shenoy, G.K., Wagner, F.E., and Kalvius, G.M. (1978) The measurement of the isomer shift. In  
794 G.K. Schenoy and F.E. Wagner, Eds., *Mössbauer Isomer Shifts*, p. 49-110. Amsterdam: North-  
795 Holland Publishing Co.
- 796 Toby, B.H. and Von Dreele, R.B. (2013) GSAS-II: the genesis of a modern open-source all purpose  
797 crystallography software package. *Journal of Applied Crystallography*, 46(2), 544-549.
- 798 Ulrych, J., Povondra, P., Pivec, E., Rutšek, J., and Sitek, J. (1994) Compositional evolution of  
799 metasomatic garnet in melilitic rocks of the Osečná complex, Bohemia. *Canadian Mineralogist*,  
800 32, 637-647.
- 801 Ungaretti, L., Leona, M., Merli, M., and Oberti, R. (1995) Non-ideal solid-solution in garnet:  
802 crystal-structure evidence and modelling. *European Journal of Mineralogy*, 7, 1299-1312.
- 803 Valley, J.W., Essene, E.J., and Peacor, D.R. (1983) Fluorine-bearing garnets in Adirondack calc-  
804 silicates. *American Mineralogist*, 68, 444-448.
- 805 Visser, D. (1993) Fluorine-bearing hydrogarnets from Blengsvatn, Bamble sector, south Norway.  
806 *Mineralogy and Petrology*, 47, 209-218.
- 807 Wang, Y. and Lai, W. (2012) High ionic conductivity lithium garnet oxides of  $\text{Li}_{7-x}\text{La}_3\text{Zr}_{2-x}\text{Ta}_x\text{O}_{12}$   
808 compositions. *Electrochemical and Solid-State Letters*, 15(5), A68-A71.

- 809 Watkin, D. (2008) Structure refinement: some background theory and practical strategies. *Journal*  
810 *of Applied Crystallography*, 41, 491-522.
- 811 Waychunas, G.A. (1987) Synchrotron radiation XANES spectroscopy of Ti in minerals: Effects of  
812 Ti bonding distances, Ti valence, and site geometry on absorption edge structure. *American*  
813 *Mineralogist*, 72, 89-101.
- 814 Wood, B.J., Kiseeva, E.S., and Matzen, A.K. (2013) Garnet in the Earth's mantle. *Elements*, 9, 421-  
815 426.
- 816 Yang, H., Konzett, J., Downs, R.T., and Frost, D.J. (2009) Crystal structure and Raman spectrum of  
817 a high-pressure Li-rich majoritic garnet,  $(\text{Li}_2\text{Mg})\text{Si}_2(\text{SiO}_4)_3$ . *American Mineralogist*, 94, 630-  
818 633.
- 819 Young, R.A., Ed. (1993) *The Rietveld method*, 308 p. International Union of Crystallography,  
820 Oxford Science Publications.

821

822

## 823 **FIGURE CAPTIONS**

- 824 **FIGURE 1.** Plot of the  $\text{TiO}_2$  (wt%) vs. measured  $\text{H}_2\text{O}$  (wt%) in Ti-garnets. Symbols: solid squares  
825 = samples of this work; open symbols = samples from literature (circle: 80802 and 80303 from  
826 Onuki et al. (1982); pointing downward triangle: SB-3 from Lager et al. (1989); pointing upward  
827 triangle: SA12 from Müntener and Hermann (1994); diamond: 31/B from Ulrych et al. (1994);  
828 circle with horizontal line: Ice River crystal from Locock et al. (1995); pointing downward triangle  
829 with horizontal line: AF-05 from Chakhmouradian and McCammon (2005); pointing upward  
830 triangle with horizontal line: M-1 from Katerinopoulou et al. (2009); diamond with horizontal line:  
831 KPK39-1-1, KPK54-10, KPK54-11, KTK05, KTK07, KTK09, KTK10, KPK56-12-2, KPK56-12-9,  
832 KPN09, KPN10, KPN11 from Phichaikamjornwut et al. (2011)).
- 833 **FIGURE 2.** Room temperature Mössbauer spectra of samples W6 (a) and W16 (b).

834 **FIGURE 3.** Comparison between  $\text{Fe}^{3+}/\Sigma\text{Fe}$  as determined by Mössbauer spectroscopy and Flank  
835 method. The 1:1 line is shown. The error bars for  $\text{Fe}^{3+}/\Sigma\text{Fe}$  correspond respectively to  $\sigma = 3\%$  for  
836 the Flank method (Malaspina et al. 2012) and  $\sigma = 3\%$ , the latter being the maximum error for  
837 Mössbauer data (Dyar et al. 2008).

838 **FIGURE 4.** XRD patterns of the W6, W12, W16 and NZALA samples.

839 **FIGURE 5.** Splitting of selected diffraction peaks, (004) and (024), from the patterns in **Figure 4**.

840 **FIGURE 6.** Plot of  $a$  cell parameter vs.  $\text{TiO}_2$  (wt%) in Ti-garnets. Symbols as in **Figure 1**. In  
841 addition, circle with vertical line indicates the Magnet Cove andradite from Antao (2013).

842 **FIGURE 7.** Plot of  $a$  cell parameter vs.  $\langle\text{X-O}\rangle$  (**a**), Y-O (**b**) and Z-O (**c**) distances of Ti-garnets.  
843 Symbols as in **Figure 6**.

844 **FIGURE 8.** Plot of tetrahedral angle variance (TAV parameter) vs.  $(\text{Fe}^{2+}+\text{Al}+\text{Fe}^{3+}+\text{Ti})$  amount in  
845 the tetrahedral site of Ti-garnets and natural end-member garnets. Symbols as in **Figure 6**. Other  
846 symbols: circle with cross inside = Novak and Gibbs (1971); square with cross inside = Scordari et  
847 al. (1999); pointing downward triangle with cross inside = Schingaro et al. 2001; pointing upward  
848 triangle with cross inside = Adamo et al. (2011); diamond with cross inside = Antao (2014).

849 **FIGURE 9.** Plot of octahedral angle variance (OAV parameter) vs.  $(\text{Ti}^{4+}+\text{Zr}+\text{Fe}^{2+}+\text{Mg}+\text{Mn}+\text{Ca})$   
850 amount in the octahedral site of Ti-garnets and natural end-member garnets. Symbols as in **Figure**  
851 **8**.

852 **FIGURE 10.** Classification diagram for the studied and selected literature hydrogarnets. Symbols  
853 as in **Figure 8**. Grey symbols indicate the studied samples whose formulae have been calculated  
854 according to Grew et al. (2013). In addition, square with horizontal line represents GA34, GRR134,  
855 GRR169, GRR684, GRR1328, GRR1765, GA32, GA35, GRR149, GRR1015, GRR1447, GA24,  
856 GA36, GRR1446, CITH3110 samples from Amthauer and Rossman (1998).

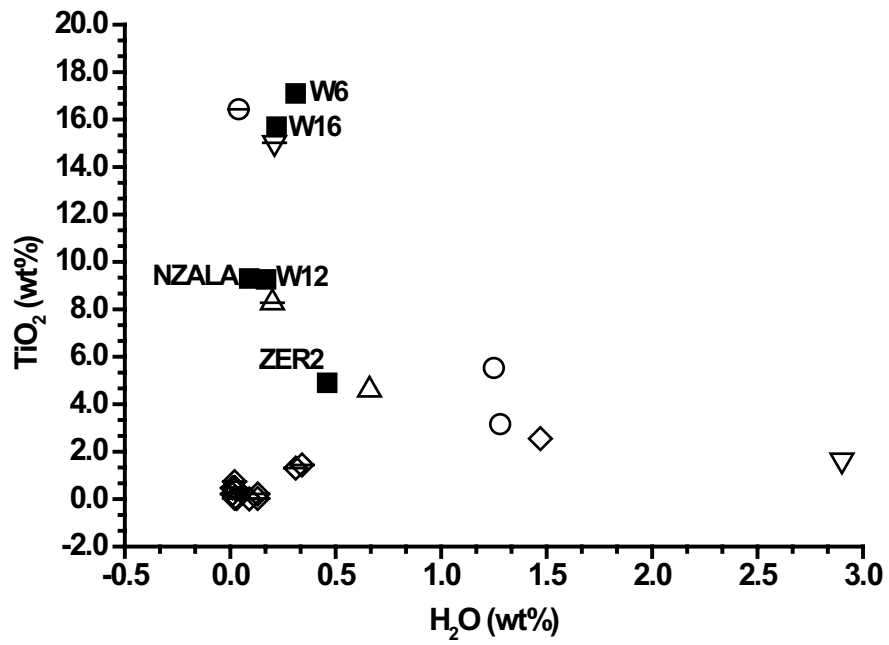


Figure 1

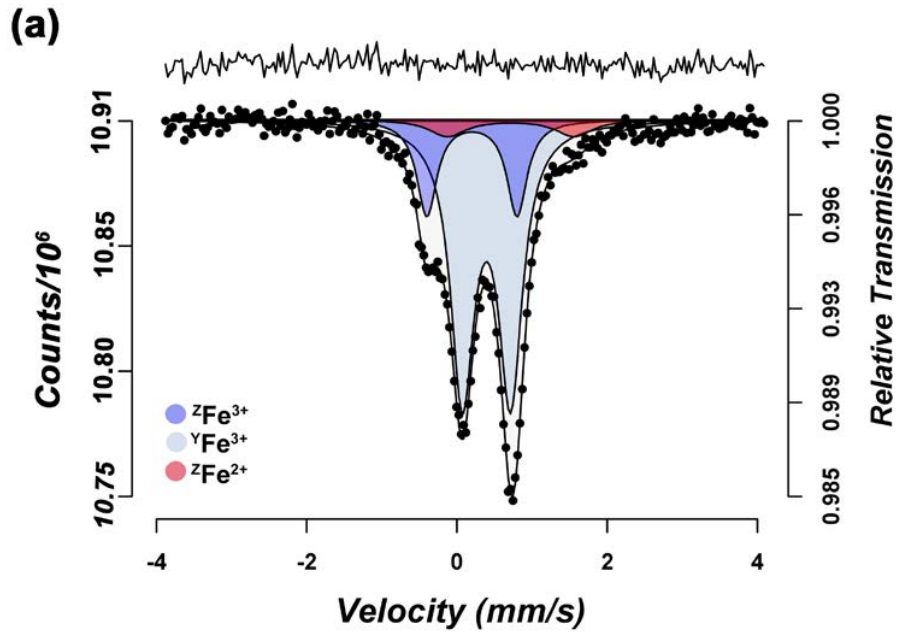


Figure 2a

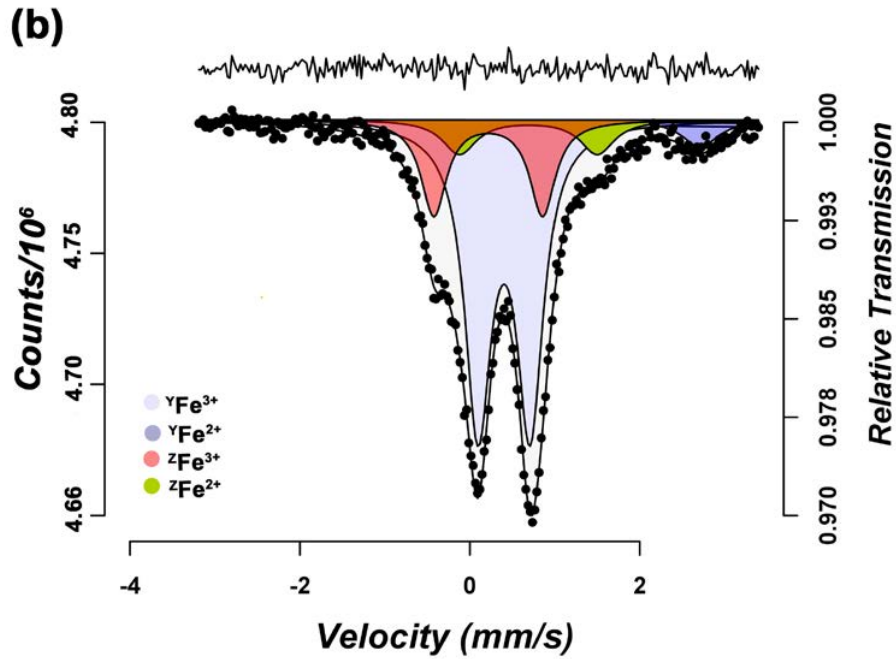


Figure 2b

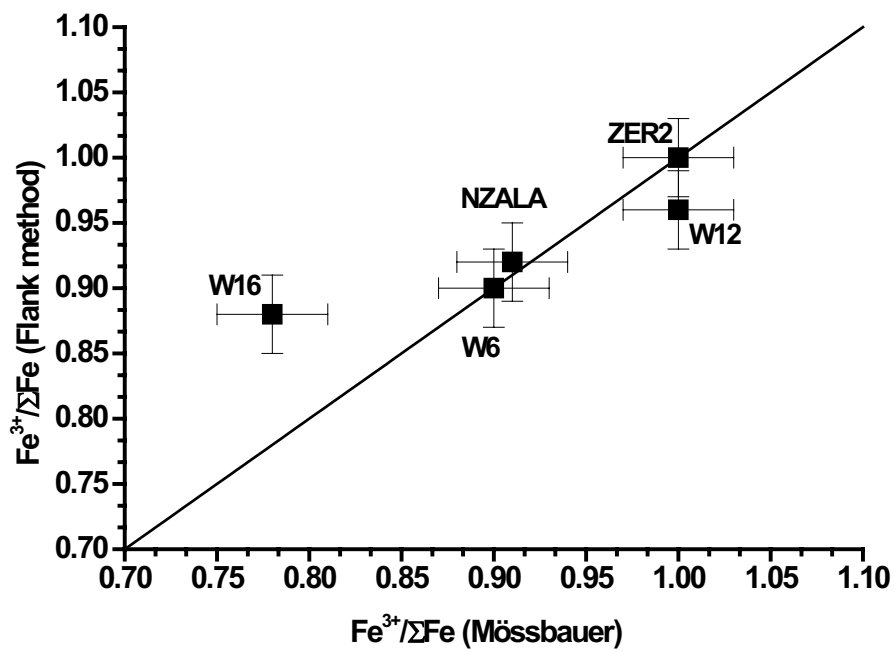


Figure 3

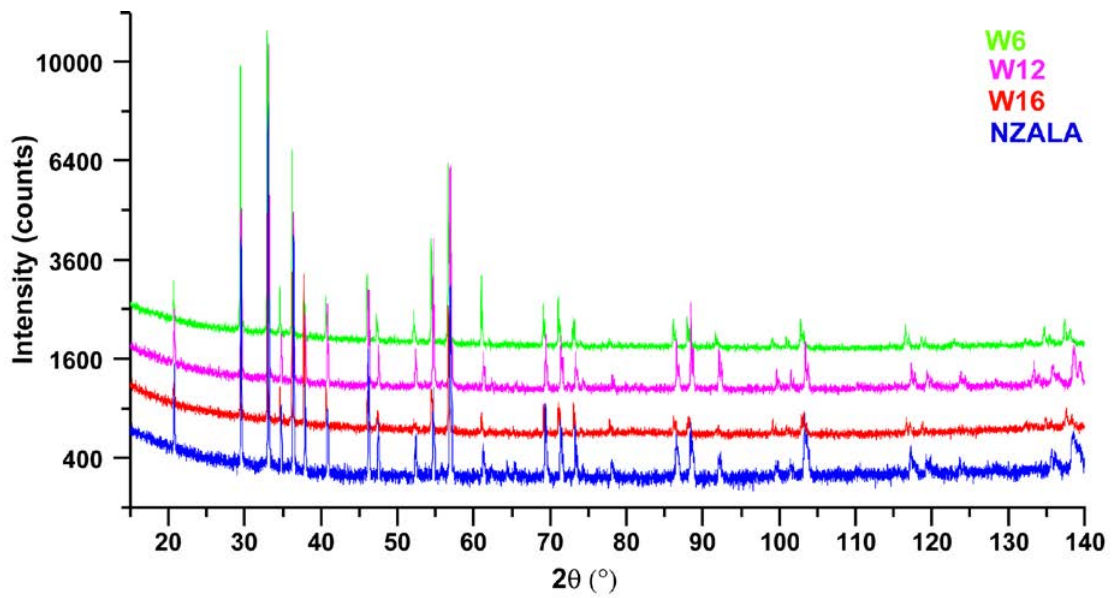


Figure 4

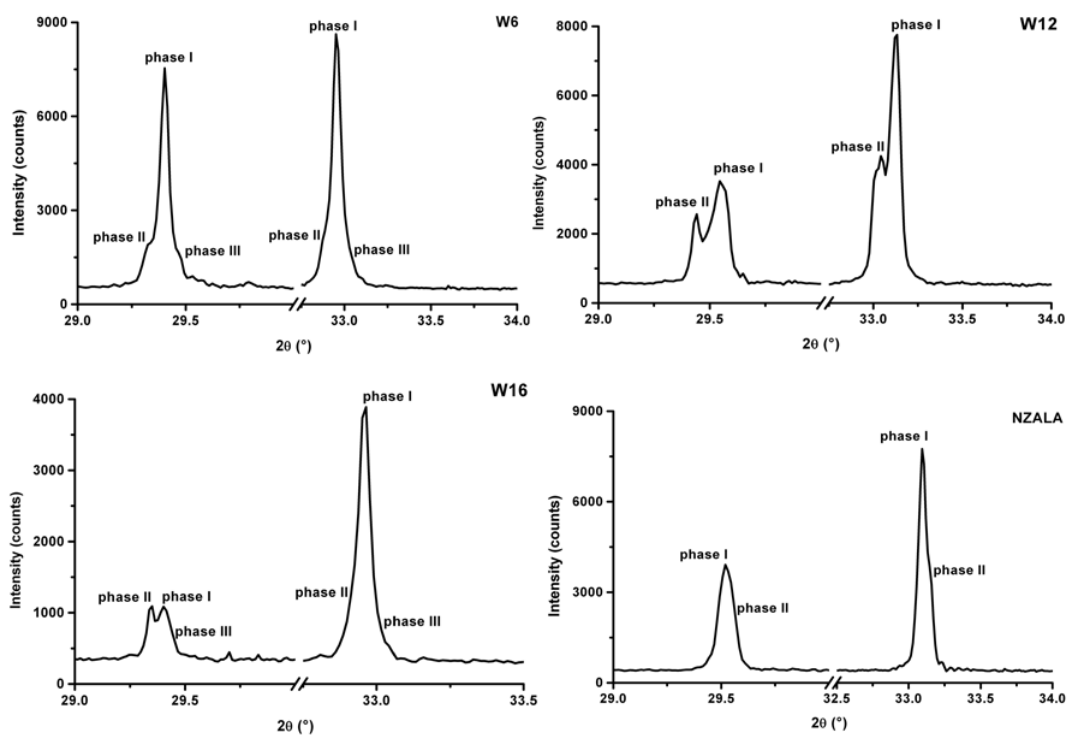


Figure 5

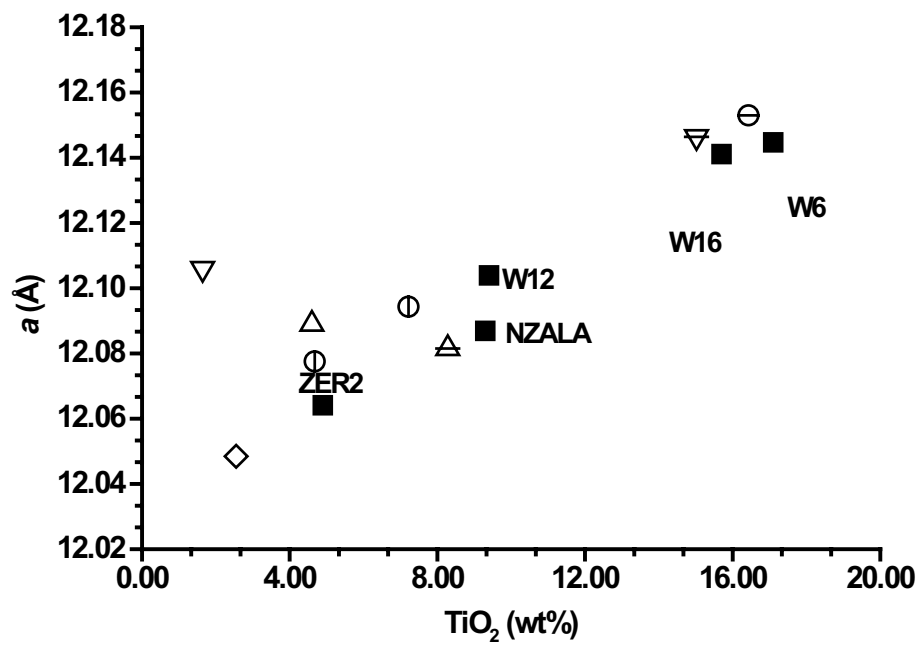


Figure 6

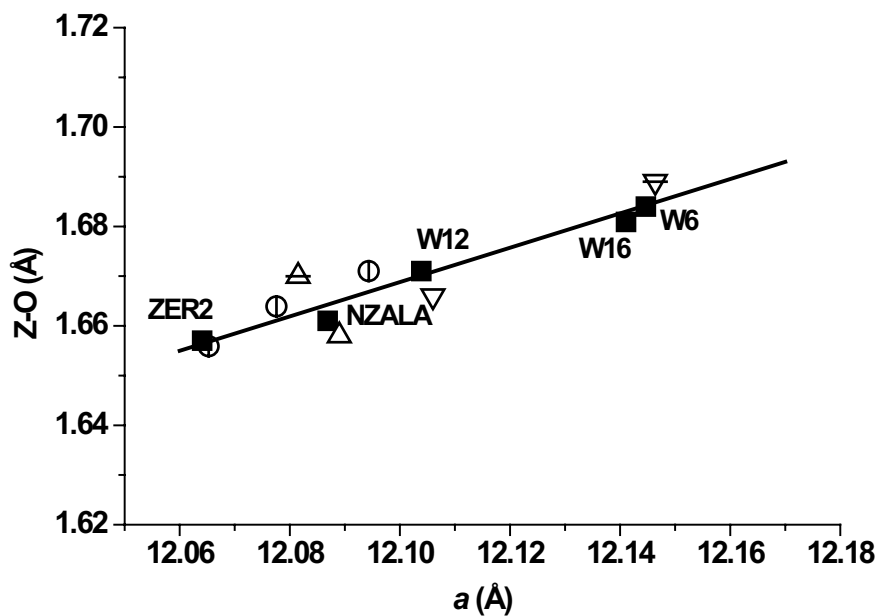


Figure 7a

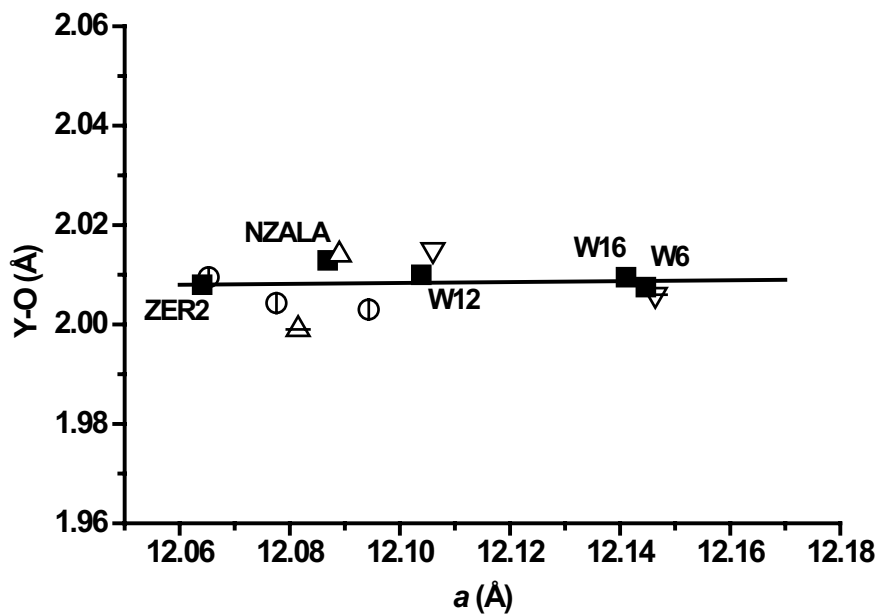


Figure 7b

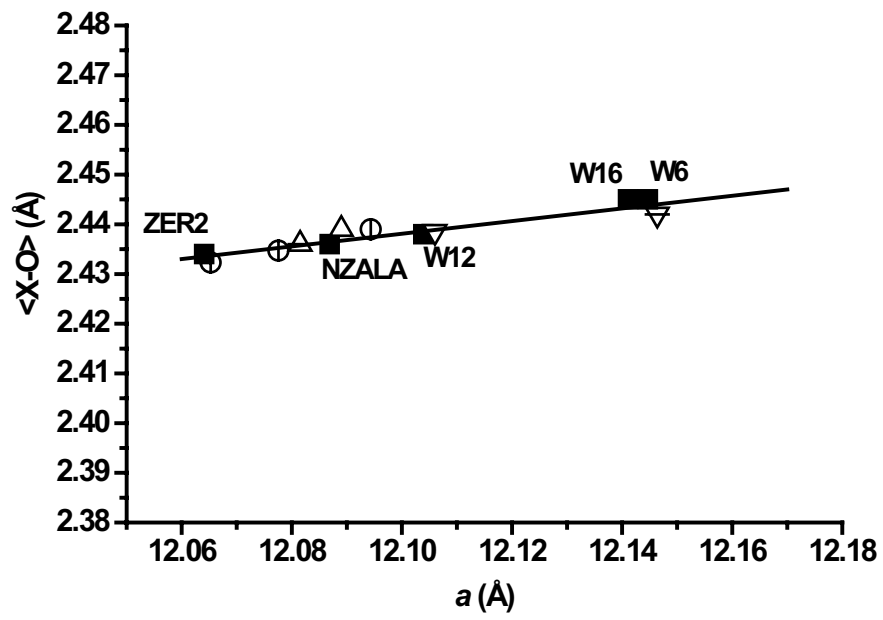


Figure 7c

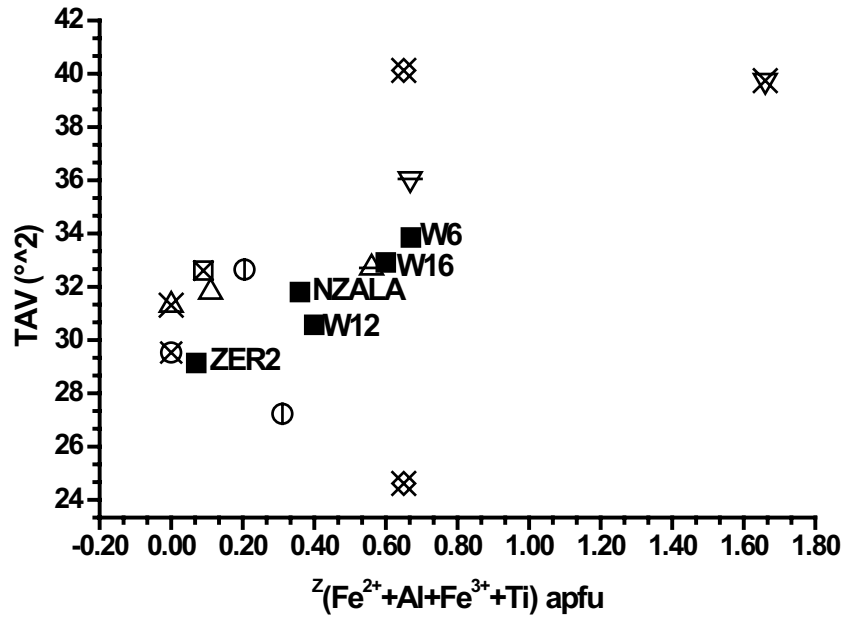


Figure 8

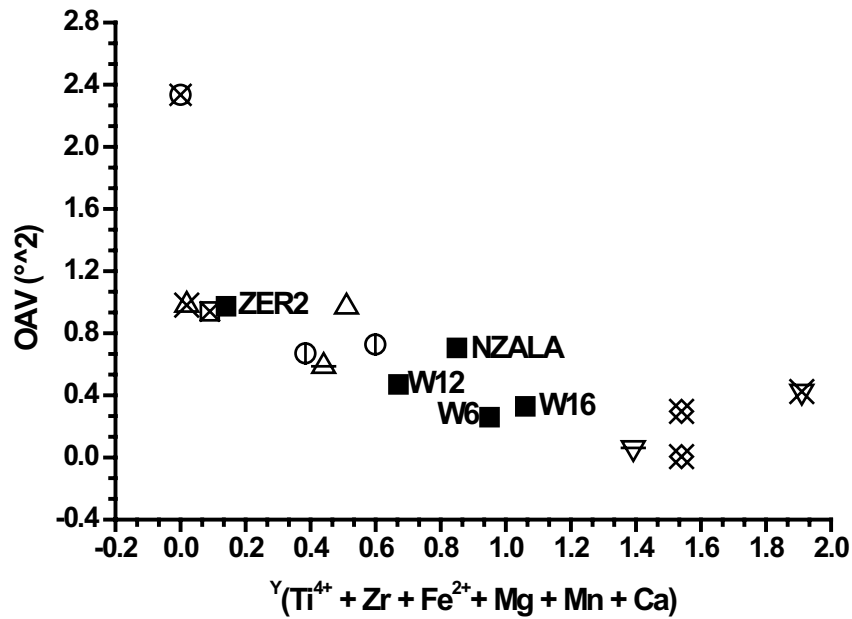


Figure 9

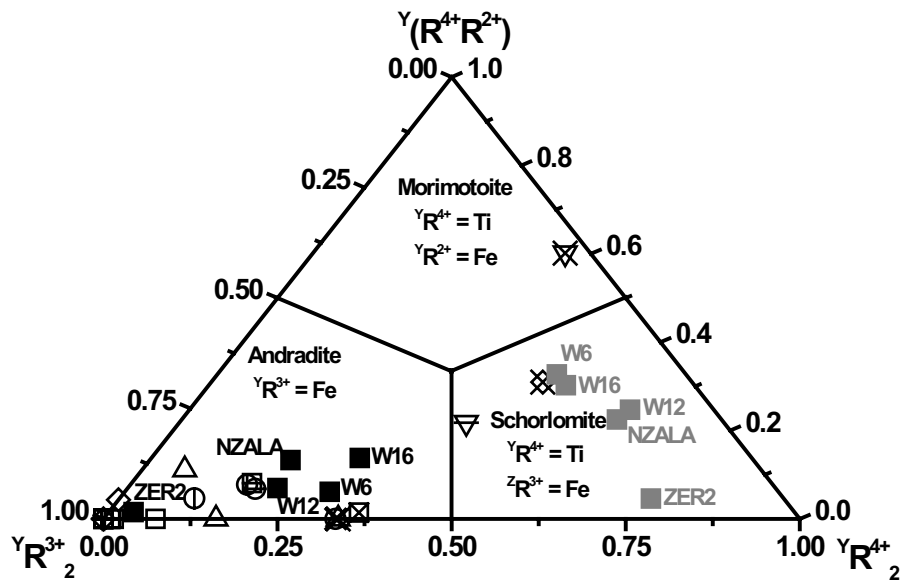


Figure 10

**Table 1.** Origin, provenance and literature data of the analysed samples.

<b>Label</b>	<b>Provenance</b>	<b>References</b>
<b>Magmatic alkaline rocks</b>		
W6	Iivaara, Finland	Howie and Woolley (1968)
W16	Rusinga Island, Kenya	Howie and Woolley (1968)
<b>Carbonatitic rocks</b>		
W12	Magnet Cove, Arkansas	Howie and Woolley (1968); Pedrazzi et al. (2002)
<b>Metamorphic rocks</b>		
NZALA	Atlas mountains, Marocco	Armbruster et al. (1998); Pedrazzi et al. (2002)
ZER2	Zermatt, Switzerland	Armbruster et al. (1998); Pedrazzi et al. (2002)

**Table 2.** Chemical composition (wt%) of the studied garnets.

	<b>W6</b>	<b>W12</b>	<b>W16</b>	<b>NZALA</b>	<b>ZER2</b>
<b>CaO</b>	31.7(1)	32.2(1)	31.5(1)	31.9(1)	33.2(1)
<b>Na<sub>2</sub>O</b>	0.31(2)	0.05(3)	0.35(2)	0.14(2)	0.01(1)
<b>MgO</b>	1.20(2)	0.99(1)	0.95(3)	0.75(2)	0.44(3)
<b>MnO</b>	0.21(2)	0.26(3)	0.33(2)	0.51(2)	0.23(3)
<b>FeO</b>	19.3(2)	20.1(1)	19.7(2)	20.8(3)	20.9(2)
<b>Al<sub>2</sub>O<sub>3</sub></b>	0.96(2)	2.08(4)	1.0(1)	1.17(4)	2.5(1)
<b>ZrO<sub>2</sub></b>	0.18(2)	0.01(1)	0.37(3)	0.2(1)	0.15(1)
<b>TiO<sub>2</sub></b>	17.1(2)	9.26(2)	15.7(1)	9.3(3)	4.9(1)
<b>Cr<sub>2</sub>O<sub>3</sub></b>	0.02(1)	0.02(2)	0.01(1)	0.07(3)	0.13(4)
<b>SiO<sub>2</sub></b>	27.0(1)	29.9(1)	27.9(1)	30.4(2)	34.5(4)
<b>Total</b>	98.0(2)	94.9(3)	97.8(2)	95.2(4)	97.0(4)
<b>H<sub>2</sub>O<sup>†</sup></b>	0.31(3)	0.17(1)	0.22(3)	0.091(7)	0.46(4)
<b>Li<sub>2</sub>O<sup>†</sup></b>	0.004(2)	0.0038(2)	0.011(6)	0.008(1)	0.014(2)
<b>F<sup>†</sup></b>	0.009(4)	0.011(2)	0.040(4)	0.020(1)	0.004(1)
<b>Fe<sup>3+</sup>/ΣFe*</b>	0.90(1)	0.96(1)	0.88(2)	0.92(1)	1.00(1)
<b>Fe<sup>3+</sup>/ΣFe**</b>	0.79	0.96	0.79	0.92	0.86

*Note:*<sup>†</sup>SIMS data; \*from Flank method; \*\*calculated on the basis of the charge balance according to Grew et al. 2013 (see details in the text).

**Table 3.** Mössbauer parameters of W6 and W16 garnets as obtained by Lorentzian fitting and corrected according to Dyar et al. (2012). Literature data on W12, NZALA and ZER2 samples (Pedrazzi et al. 2002) are also reported.

	$\chi^2_r$	Site	Species	IS (mm/s)	QS (mm/s)	$\Gamma$ (mm/s)	A(%)
		Y	Fe <sup>3+</sup>	0.393(6)	0.64(1)	0.38(1)	70(1)
<b>W6</b>	0.93	Z	Fe <sup>3+</sup>	0.20(1)	1.20(5)	0.32(4)	20(1)
		Z	Fe <sup>2+</sup>	0.7(2)	1.7(7)	0.6(2)	10(2)
		Y	Fe <sup>3+</sup>	0.402(4)	0.61(1)	0.37(8)	59(1)
		Y	Fe <sup>2+</sup>	1.3(7)	2.8(3)	0.52(6)	10(2)
<b>W16</b>	1.40	Z	Fe <sup>3+</sup>	0.22(1)	1.28(6)	0.37(3)	19(3)
		Z	Fe <sup>2+</sup>	0.7(6)	1.6(8)	0.46(6)	12(2)
<b>W12*</b>	1.29	Y	Fe <sup>3+</sup>	0.399(5)	0.617(6)	0.326(5)	81(3)
		Z	Fe <sup>3+</sup>	0.221(2)	1.208(4)	0.401(4)	19(2)
<b>NZALA*</b>	1.11	Y	Fe <sup>3+</sup>	0.402(5)	0.597(5)	0.331(6)	79(7)
		Z	Fe <sup>3+</sup>	0.208(1)	1.253(3)	0.318(4)	12(7)
		Z	Fe <sup>2+</sup>	0.70(1)	1.66(1)	0.25(9)	4(2)
		Y	Fe <sup>2+</sup>	1.28(8)	2.91(2)	0.48(2)	5(3)
<b>ZER2*</b>	1.16	Y	Fe <sup>3+</sup>	0.399(1)	0.582(3)	0.312(4)	100

Notes:  $\chi^2_r$  = reduced  $\chi^2 = \chi^2/\text{degrees of freedom}$ ; \*data from Pedrazzi et al. (2002).

**Table 4.** Powder and single crystal X-ray diffraction data of the studied garnets.

	<b>W6</b>		<b>W12</b>		<b>W16</b>		<b>NZALA</b>		<b>ZER2</b>	
<b>XRPD data</b>										
	phase I	phase II	phase I	phase II						
<b>Weight fraction (%)</b>	66(3)	34(3)	58(2)	42(2)	81(2)	19(2)	80(2)	20(1)		
<b><i>a</i> (Å)</b>	12.1476(2)	12.1599(9)	12.0948(3)	12.1156(7)	12.1459(2)	12.1648(9)	12.1045(2)	12.0883(3)		
<b>N<sub>obs</sub></b>	148	148	146	148	148	148	148	146		
<b>Data points</b>	10383		10383		10383		10383			
<b>wR (%)</b>	10.45		11.54		10.49		10.12			
<b>SCXRD data</b>										
<b>Crystal size (mm<sup>3</sup>)</b>	0.60x0.58x0.23		0.48x0.24x0.16		0.56x0.33x0.07		0.60x0.50x0.14		0.51x0.22x0.11	
<b>Space group</b>	<i>Ia</i> $\bar{3}$ <i>d</i>		<i>Ia</i> $\bar{3}$ <i>d</i>							
<b><i>a</i> (Å)</b>	12.1447(1)		12.1039(1)		12.1411(1)		12.0869(2)		12.0641(1)	
<b>Cell volume (Å<sup>3</sup>)</b>	1791.27(3)		1773.27(3)		1789.67(3)		1765.81(5)		1755.84(3)	
<b>Z</b>	8		8		8		8		8	
<b>θ range for data collection</b>	4 to 36°		5 to 30°		4 to 36°		5 to 36°		4 to 36°	
<b>Reflections collected</b>	20828		14993		20821		20402		20641	
<b>Reflections unique</b>	366		228		366		363		362	
<b>R<sub>merging</sub> [R<sub>(int)</sub>] (%)</b>	2.20		2.20		1.93		3.47		1.77	
<b>Reflections used (<i>I</i>&gt;3σ(<i>I</i>))</b>	332		206		341		323		334	
<b>No. of refined parameters</b>	21		21		21		21		19	
<b>Goof*</b>	1.08		0.92		1.02		0.94		0.87	
<b>R<sub>1</sub><sup>†</sup> [on <i>F</i>] (%)</b>	2.00		1.78		1.95		1.65		2.09	
<b>wR<sub>2</sub><sup>‡</sup> [on <i>F</i><sup>2</sup>] (%)</b>	2.94		2.38		2.55		2.35		3.02	
<b>Δρ<sub>min</sub>/Δρ<sub>max</sub> (e<sup>-</sup>/Å<sup>3</sup>)</b>	-0.40/0.49		-0.74/0.25		-0.40/0.49		-0.43/0.36		-0.96/0.34	
<i>Notes:</i> *: Goodness-of-fit = [Σ[w( <i>F</i> <sub>o</sub> <sup>2</sup> - <i>F</i> <sub>c</sub> <sup>2</sup> ) <sup>2</sup> ]/(N-p)] <sup>1/2</sup> , where <i>N</i> and <i>p</i> are the number of reflections and parameters, respectively.										
<sup>†</sup> : R <sub>1</sub> = Σ[ F <sub>o</sub>   -  F <sub>c</sub>  ]/Σ F <sub>o</sub>  .										
<sup>‡</sup> : wR <sub>2</sub> = [Σ[w( <i>F</i> <sub>o</sub> <sup>2</sup> - <i>F</i> <sub>c</sub> <sup>2</sup> ) <sup>2</sup> ]/Σ[w( <i>F</i> <sub>o</sub> <sup>2</sup> ) <sup>2</sup> ] <sup>1/2</sup> ; <i>w</i> = quasi-unit weight.										

**Table 5.** Crystallographic coordinates, site occupancies, equivalent/isotropic ( $\text{\AA}^2$ ) and anisotropic displacement parameters ( $\text{\AA}^2$ ) of the studied crystals.

Sample	Site	Atom	$x$	$y$	$z$	Occupancy	$U_{\text{iso/equiv}}$	$U_{11}$	$U_{22}$	$U_{33}$	$U_{23}$	$U_{13}$	$U_{12}$
<b>W6</b>													
	X	Ca <sup>2+</sup>	1/8	0	1/4	1.0000	0.0087	0.0063(2)	0.0099(1)	0.0099(1)	0.00252(8)	0	0
	Y	Fe <sup>3+</sup>	0	0	0	0.7304(8)	0.0049	0.0049(1)	0.0049(1)	0.0049(1)	0.00038(4)	0.00038(4)	0.00038(4)
		Al <sup>3+</sup>				0.2698(8)							
	Z	Si <sup>4+</sup>	3/8	0	1/4	0.878(1)	0.0054	0.0046(2)	0.0059(2)	0.0059(2)	0	0	0
		Fe <sup>3+</sup>				0.137(5)							
	O	O <sup>2-</sup>	0.03779(5)	0.04819(5)	0.65358(5)	1.0000	0.0102	0.0132(3)	0.0088(2)	0.0085(2)	-0.0011(2)	0.0031(2)	-0.0016(2)
<b>W12</b>													
	X	Ca <sup>2+</sup>	1/8	0	1/4	1.0000	0.0078	0.0058(2)	0.0088(2)	0.0088(2)	0.00214(9)	0	0
	Y	Fe <sup>3+</sup>	0	0	0	0.732(1)	0.0044	0.0044(2)	0.0044(2)	0.0044(2)	0.00009(5)	0.00009(5)	0.00009(5)
		Al <sup>3+</sup>				0.268(1)							
	Z	Si <sup>4+</sup>	3/8	0	1/4	0.935(2)	0.0041	0.0038(3)	0.0043(3)	0.0043(3)	0	0	0
		Fe <sup>3+</sup>				0.064(1)							
	O	O <sup>2-</sup>	0.03825(4)	0.04823(4)	0.65400(4)	1.0000	0.0078	0.0096(3)	0.0073(3)	0.0066(3)	-0.0002(2)	0.0018(2)	-0.0007(2)
<b>W16</b>													
	X	Ca <sup>2+</sup>	1/8	0	1/4	1.0000	0.0085	0.0059(1)	0.0099(1)	0.0099(1)	0.00279(9)	0	0
	Y	Fe <sup>3+</sup>	0	0	0	0.728(1)	0.0045	0.0045(1)	0.0045(1)	0.0045(1)	0.00049(5)	0.00049(5)	0.00049(5)
		Al <sup>3+</sup>				0.272(1)							
	Z	Si <sup>4+</sup>	3/8	0	1/4	0.859(1)	0.0052	0.0042(2)	0.0057(2)	0.0057(2)	0	0	0
		Fe <sup>3+</sup>				0.143(5)							
	O	O <sup>2-</sup>	0.03793(5)	0.04821(5)	0.65372(5)	1.0000	0.0099	0.0130(3)	0.0087(3)	0.0080(2)	-0.0008(2)	0.0028(2)	-0.0017(2)
<b>NZALA</b>													
	X	Ca <sup>2+</sup>	1/8	0	1/4	1.0000	0.0083	0.0062(1)	0.0094(1)	0.0094(1)	0.00202(6)	0	0
	Y	Fe <sup>3+</sup>	0	0	0	0.7932(9)	0.0050	0.0050(1)	0.0050(1)	0.0050(1)	0.00015(3)	0.00015(3)	0.00015(3)
		Al <sup>3+</sup>				0.207(1)							

<b>Z</b>	<b>Si<sup>4+</sup></b>	$\frac{3}{8}$	0	$\frac{1}{4}$	0.912(1)	0.0052	0.0045(2)	0.0055(2)	0.0055(2)	0	0	0
	<b>Fe<sup>3+</sup></b>				0.071(5)							
<b>O</b>	<b>O<sup>2-</sup></b>	0.03869(4)	0.04831(4)	0.65454(4)	1.0000	0.0085	0.0098(2)	0.0084(2)	0.0072(2)	-0.0001(1)	0.0010(1)	-0.0004(1)
<b>ZER2</b>												
<b>X</b>	<b>Ca<sup>2+</sup></b>	$\frac{1}{8}$	0	$\frac{1}{4}$	1.0000	0.0064	0.0046(2)	0.0074(1)	0.0074(1)	0.00170(7)	0	0
<b>Y</b>	<b>Fe<sup>3+</sup></b>	0	0	0	0.792(1)	0.0046	0.0046(2)	0.0046(2)	0.0046(2)	0.00006(4)	0.00006(4)	0.00006(4)
	<b>Al<sup>3+</sup></b>				0.208(1)							
<b>Z</b>	<b>Si<sup>4+</sup></b>	$\frac{3}{8}$	0	$\frac{1}{4}$	1.0000	0.0049	0.0043(2)	0.0052(2)	0.0052(2)	0	0	0
<b>O</b>	<b>O<sup>2-</sup></b>	0.03899(4)	0.04825(4)	0.65457(4)	1.0000	0.0064	0.0070(2)	0.0067(2)	0.0055(2)	-0.0000(1)	0.0004(1)	-0.0002(2)

**Table 6.** Refined bond distances (Å) and distortional parameters of the studied samples, selected literature Ti-garnets and natural end-member garnets.

	Ti-andradite		Ti-andradite		Ti-Zr-Cr-rich Andradite		Ti-rich Andradite			Schorlomite	Andradite	Morimotoite		Grossular	Kimzeyite	Melanite		
	W6	W12	W16	NZALA	ZER2	Lager et al. (1989)	Müntener and Hermann (1994)	Katerinopoulou et al. (2009)	Antao (2013) Phase I	Antao (2013) Phase II	Antao (2013) Phase III	Chakhmouradian and McCammon (2005)	Adamo et al. (2011)	Antao (2014) Phase I	Antao (2014) Phase II	Novak and Gibbs (1971)	Schingaro et al. (2001)	Scordari et al. (1999)
<b>X1-O</b>	2.371(1)	2.366(1)	2.371(1)	2.364(1)	2.362(1)	2.369(1)	2.365(1)	2.361(1)	2.3609(8)	2.373(1)	2.3575(8)	2.368(1)	2.3609(7)	2.3631(9)	2.338(3)	2.325(1)	2.409(2)	2.347(1)
<b>X2-O</b>	2.518(1)	2.510(1)	2.517(1)	2.508(1)	2.505(1)	2.508(1)	2.512(1)	2.510(1)	2.5085(9)	2.505(1)	2.5070(8)	2.515(1)	2.5009(6)	2.5134(9)	2.515(3)	2.482(1)	2.546(2)	2.498(1)
<b>&lt;X-O&gt;</b>	2.445(1)	2.438(1)	2.444(1)	2.436(1)	2.434(1)	2.439(1)	2.439(1)	2.436(1)	2.4347(9)	2.439(1)	2.4323(8)	2.442(1)	2.4309(7)	2.4383(9)	2.427(3)	2.404(1)	2.478(2)	2.423(1)
<b>Y-O</b>	2.008(1)	2.008(1)	2.010(1)	2.0121(4)	2.009(1)	2.015(1)	2.014(1)	1.999(1)	2.0043(9)	2.003(1)	2.0095(9)	2.006(1)	2.0199(6)	2.011(1)	1.988(3)	1.924(1)	2.050(2)	1.989(1)
<b>Z-O</b>	1.684(1)	1.671(1)	1.681(1)	1.6615(4)	1.656(1)	1.666(1)	1.658(1)	1.670(1)	1.6639(9)	1.671(1)	1.6559(9)	1.689(1)	1.6474(6)	1.693(1)	1.704(3)	1.645(1)	1.738(2)	1.651(1)
<b>&lt;D-O&gt; [Å]</b>	2.145	2.139	2.145	2.136	2.131	2.140	2.137	2.135	2.134	2.138	2.132	2.145	2.132	2.145	2.136	2.094	2.186	2.121
<b>Volume<sub>x</sub> [Å<sup>3</sup>]</b>	25.019	24.759	25.001	24.705	24.616	24.781	24.790	24.731	24.697	24.773	24.623	24.933	24.528	24.856	25.165	23.800	26.012	24.316
<b>Δ(X-O)</b>	0.147	0.138	0.145	0.143	0.137	0.139	0.146	0.149	0.148	0.133	0.149	0.148	0.140	0.15	0.127	0.1557	0.136	0.152
<b>α (°)</b>	26.518	26.851	26.603	26.888	26.847	26.950	26.771	26.429	26.594	26.710	26.745	26.584	27.213	26.803	26.168	24.871	27.368	26.331
<b>Volume<sub>y</sub> [Å<sup>3</sup>]</b>	10.786	10.816	10.818	10.873	10.791	10.904	10.885	10.652	10.733	10.718	10.815	10.766	10.983	10.847	10.478	9.528	11.507	10.473
<b>OAV [°^2]</b>	0.259	0.47	0.329	0.705	0.973	0.579	0.969	0.580	0.670	0.727	0.800	0.062	0.981	0.005	0.297	2.335	0.424	0.94
<b>S(Y) [Å]</b>	2.851	2.858	2.855	2.867	2.863	2.868	2.871	2.845	2.854	2.853	2.863	2.843	2.880	2.843	2.825	2.754	2.885	2.834
<b>U(Y) [Å]</b>	2.827	2.825	2.828	2.827	2.816	2.831	2.824	2.809	2.815	2.813	2.820	2.831	2.833	2.846	2.799	2.695	2.917	2.789
<b>t<sub>sv</sub> [Å]</b>	2.298	2.294	2.298	2.292	2.280	2.297	2.287	2.279	2.283	2.280	2.285	2.307	2.293	2.325	2.275	2.175	2.394	2.258
<b>t<sub>vy</sub> [Å]</b>	2.338	2.347	2.343	2.357	2.357	2.356	2.363	2.338	2.346	2.346	2.355	2.326	2.371	2.320	2.317	2.273	2.343	2.333
<b>X-Y [Å]</b>	3.395	3.383	3.394	3.378	3.372	3.384	3.379	3.377	3.376	3.380	3.372	3.395	3.371	3.398	3.399	3.314	3.464	3.354
<b>φ(°)</b>	133.55	133.42	133.53	133.49	133.64	133.39	133.70	133.81	133.72	133.66	133.64	133.30	133.34	132.87	133.89	135.51	132.00	134.04
<b>Volume<sub>z</sub> [Å<sup>3</sup>]</b>	2.42	2.368	2.408	2.324	2.31	2.348	2.312	2.358	2.336	2.370	2.301	2.441	2.268	2.455	2.516	2.289	2.656	2.286
<b>TAV [°^2]</b>	33.847	30.567	32.915	31.801	29.135	31.102	31.803	32.615	32.648	27.230	33.657	36.048	31.309	40.124	24.615	27.066	39.742	32.610
<b>S(Z) [Å]</b>	2.618	2.605	2.615	2.587	2.586	2.596	2.582	2.598	2.589	2.612	2.575	2.622	2.566	2.621	2.669	2.582	2.691	2.571
<b>U(Z) [Å]</b>	2.813	2.789	2.807	2.773	2.764	2.781	2.768	2.788	2.779	2.785	2.766	2.824	2.750	2.835	2.837	2.753	2.909	2.759
<b>t<sub>sz</sub> [Å]</b>	2.118	2.094	2.112	2.085	2.073	2.089	2.081	2.097	2.090	2.085	2.083	2.130	2.066	2.145	2.118	2.060	2.201	2.075
<b>t<sub>z</sub> [Å]</b>	1.851	1.842	1.849	1.829	1.828	1.836	1.826	1.837	1.831	1.847	1.821	1.854	1.815	1.853	1.887	1.826	1.903	1.818
<b>X-Z [Å]</b>	3.036	3.026	3.035	3.022	3.016	3.027	3.022	3.020	3.019	3.024	3.016	3.037	3.015	3.039	3.040	2.964	3.099	3.000

Notes: <D-O> = [(Z-O) + (Y-O) + (X1-O) + (X2-O)]/4 according to Antao (2013); Volume of X, Y and Z sites calculated using the IVTON software (Balic Zunic and Vickovic 1996); Δ(X-O) = (X2-O)-(X1-O) (Ungaretti et al. 1995); α: tetrahedral rotation along the  $\bar{4}$  axis (Born and Zemann 1964); TAV and OAV: tetrahedral and octahedral, respectively, angle variance (Robinson et al. 1971); S(Y) and S(Z) stand for shared edges of octahedra and tetrahedra, respectively; U(Y) and U(Z) stand for unshared edges of octahedra and tetrahedra, respectively; t<sub>sv</sub> and t<sub>sz</sub>: the distance between shared edges of octahedra and tetrahedra, respectively; t<sub>vy</sub> and t<sub>z</sub>: the distance between unshared edges of octahedra and tetrahedra, respectively; X-Y and X-Z: interatomic distance between the X cation and Y, and Z cation, respectively; φ: Si-O-Y angle (Yang et al. 2009).

**Table 7.** Structural formulae in atoms per formula unit (apfu) of the studied samples, selected literature Ti-garnets and natural end-member garnets.

	X site	Y site	Z site	φ site	SIMS data
<b>Cation distribution from this study:</b>					
<b>W6</b>	(Ca <sub>2.88</sub> Mg <sub>0.07</sub> Na <sub>0.05</sub> )Σ=3.00	(Mg <sub>0.08</sub> Mn <sub>0.02</sub> Fe <sup>3+</sup> <sub>0.88</sub> Ti <sup>3+</sup> <sub>0.17</sub> Ti <sup>4+</sup> <sub>0.84</sub> Zr <sub>0.01</sub> )Σ=2.00	(Si <sub>2.29</sub> Ti <sub>0.08</sub> Fe <sup>3+</sup> <sub>0.38</sub> Fe <sup>2+</sup> <sub>0.11</sub> Al <sub>0.10</sub> []) <sub>0.04</sub> Σ=3.00	O <sub>11.84</sub> OH <sub>0.16</sub>	OH <sub>0.17</sub> F <sub>0.002</sub> Li <sub>0.001</sub>
<b>W12</b>	(Ca <sub>2.98</sub> Mn <sub>0.01</sub> Na <sub>0.01</sub> )Σ=3.00	(Mg <sub>0.13</sub> Fe <sup>3+</sup> <sub>1.18</sub> Al <sub>0.09</sub> Ti <sup>3+</sup> <sub>0.06</sub> Ti <sup>4+</sup> <sub>0.54</sub> )Σ=2.00	(Si <sub>2.58</sub> Fe <sup>3+</sup> <sub>0.28</sub> Al <sub>0.12</sub> []) <sub>0.02</sub> Σ=3.00	O <sub>11.92</sub> OH <sub>0.08</sub>	OH <sub>0.10</sub> F <sub>0.003</sub> Li <sub>0.001</sub>
<b>W16</b>	(Ca <sub>2.88</sub> Mg <sub>0.06</sub> Na <sub>0.06</sub> )Σ=3.00	(Mg <sub>0.06</sub> Mn <sub>0.02</sub> Fe <sup>2+</sup> <sub>0.15</sub> Fe <sup>3+</sup> <sub>0.73</sub> Al <sub>0.10</sub> Ti <sup>3+</sup> <sub>0.11</sub> Ti <sup>4+</sup> <sub>0.81</sub> Zr <sub>0.02</sub> )Σ=2.00	(Si <sub>2.38</sub> Ti <sub>0.08</sub> Fe <sup>3+</sup> <sub>0.50</sub> Fe <sup>2+</sup> <sub>0.02</sub> []) <sub>0.02</sub> Σ=3.00	O <sub>11.92</sub> OH <sub>0.07</sub> F <sub>0.01</sub>	OH <sub>0.12</sub> F <sub>0.010</sub> Li <sub>0.001</sub>
<b>NZALA</b>	(Ca <sub>2.96</sub> Mg <sub>0.02</sub> Na <sub>0.02</sub> )Σ=3.00	(Mg <sub>0.07</sub> Mn <sub>0.04</sub> Fe <sup>2+</sup> <sub>0.12</sub> Fe <sup>3+</sup> <sub>1.09</sub> Cr <sub>0.01</sub> Al <sub>0.05</sub> Ti <sup>4+</sup> <sub>0.61</sub> Zr <sub>0.01</sub> )Σ=2.00	(Si <sub>2.64</sub> Fe <sup>3+</sup> <sub>0.29</sub> Al <sub>0.06</sub> Fe <sup>2+</sup> <sub>0.01</sub> )Σ=3.00	O <sub>12.00</sub>	OH <sub>0.05</sub> F <sub>0.005</sub> Li <sub>0.003</sub>
<b>ZER2</b>	(Ca <sub>2.97</sub> Mg <sub>0.03</sub> Li <sub>0.01</sub> )Σ=3.01	(Mg <sub>0.02</sub> Mn <sub>0.01</sub> Fe <sup>3+</sup> <sub>1.46</sub> Cr <sub>0.01</sub> Al <sub>0.18</sub> Ti <sup>3+</sup> <sub>0.21</sub> Ti <sup>4+</sup> <sub>0.10</sub> Zr <sub>0.01</sub> )Σ=2.00	(Si <sub>2.88</sub> Al <sub>0.07</sub> []) <sub>0.05</sub> Σ=3.00	O <sub>11.80</sub> OH <sub>0.20</sub>	OH <sub>0.25</sub> F <sub>0.001</sub> Li <sub>0.005</sub>
<b>Cation distribution after Grew et al. (2013):</b>					
<b>W6</b>	(Ca <sub>2.88</sub> Fe <sub>0.05</sub> Mn <sub>0.02</sub> Na <sub>0.05</sub> )Σ=3.00	(Mg <sub>0.15</sub> Fe <sup>2+</sup> <sub>0.23</sub> Fe <sup>3+</sup> <sub>0.52</sub> Ti <sub>1.09</sub> Zr <sub>0.01</sub> )Σ=2.00	(Si <sub>2.29</sub> Fe <sup>3+</sup> <sub>0.57</sub> Al <sub>0.10</sub> )Σ=2.96	O <sub>11.82</sub> OH <sub>0.18</sub>	
<b>W12</b>	(Ca <sub>2.98</sub> Mn <sub>0.02</sub> Na <sub>0.01</sub> )Σ=3.01	(Mg <sub>0.13</sub> Fe <sup>2+</sup> <sub>0.06</sub> Fe <sup>3+</sup> <sub>1.20</sub> Ti <sub>0.60</sub> )Σ=1.99	(Si <sub>2.58</sub> Fe <sup>3+</sup> <sub>0.18</sub> Al <sub>0.21</sub> )Σ=2.97	O <sub>11.90</sub> OH <sub>0.10</sub>	
<b>W16</b>	(Ca <sub>2.87</sub> Fe <sub>0.05</sub> Mn <sub>0.02</sub> Na <sub>0.06</sub> )Σ=3.00	(Mg <sub>0.12</sub> Fe <sup>2+</sup> <sub>0.24</sub> Fe <sup>3+</sup> <sub>0.62</sub> Ti <sub>1.00</sub> Zr <sub>0.02</sub> )Σ=2.00	(Si <sub>2.37</sub> Fe <sup>3+</sup> <sub>0.49</sub> Al <sub>0.10</sub> )Σ=2.96	O <sub>11.86</sub> OH <sub>0.13</sub> F <sub>0.01</sub>	
<b>NZALA</b>	(Ca <sub>2.96</sub> Mn <sub>0.02</sub> Na <sub>0.02</sub> )Σ=3.00	(Mg <sub>0.10</sub> Mn <sub>0.02</sub> Fe <sup>2+</sup> <sub>0.12</sub> Fe <sup>3+</sup> <sub>1.15</sub> Cr <sub>0.01</sub> Ti <sub>0.61</sub> Zr <sub>0.01</sub> )Σ=2.02	(Si <sub>2.63</sub> Fe <sup>3+</sup> <sub>0.24</sub> Al <sub>0.12</sub> )Σ=2.99	O <sub>11.94</sub> OH <sub>0.05</sub> F <sub>0.01</sub>	
<b>ZER2</b>	(Ca <sub>2.96</sub> Fe <sub>0.02</sub> Mn <sub>0.02</sub> )Σ=3.00	(Mg <sub>0.06</sub> Fe <sup>2+</sup> <sub>0.19</sub> Fe <sup>3+</sup> <sub>1.25</sub> Al <sub>0.19</sub> Cr <sub>0.01</sub> Ti <sub>0.31</sub> Zr <sub>0.01</sub> )Σ=2.02	(Si <sub>2.87</sub> Al <sub>0.06</sub> Li <sub>0.01</sub> )Σ=2.94	O <sub>11.74</sub> OH <sub>0.26</sub>	
<b>Müntener and Hermann (1994)</b>	Ca <sub>3.00</sub>	(Fe <sup>3+</sup> <sub>1.24</sub> Fe <sup>2+</sup> <sub>0.12</sub> Mn <sub>0.01</sub> Ca <sub>0.07</sub> Cr <sub>0.02</sub> Al <sub>0.06</sub> Ti <sup>4+</sup> <sub>0.31</sub> Ti <sup>3+</sup> <sub>0.17</sub> )Σ=2.00	(Si <sub>2.80</sub> Al <sub>0.11</sub> []) <sub>0.09</sub> Σ=3.00	O <sub>11.64</sub> OH <sub>0.36</sub>	
<b>Ulrych et al. (1994)</b>	(Ca <sub>2.904</sub> Mg <sub>0.015</sub> Mn <sub>0.003</sub> Fe <sup>2+</sup> <sub>0.024</sub> Na <sub>0.011</sub> K <sub>0.005</sub> )Σ=2.962	(Fe <sup>3+</sup> <sub>1.206</sub> Mg <sub>0.082</sub> Zr <sub>0.006</sub> Al <sub>0.551</sub> Ti <sub>0.155</sub> )Σ=2.000	(Si <sub>2.799</sub> []) <sub>0.205</sub> Σ=3.00	O <sub>11.181</sub> OH <sub>0.792</sub> F <sub>0.028</sub>	
<b>Katerinopoulou et al. (2009)</b>	(Ca <sub>2.99</sub> Mg <sub>0.03</sub> )Σ=3.02	(Fe <sup>3+</sup> <sub>0.67</sub> Cr <sub>0.54</sub> Al <sub>0.33</sub> Ti <sub>0.29</sub> Zr <sub>0.15</sub> )Σ=1.98	(Si <sub>2.42</sub> Al <sub>0.14</sub> Ti <sub>0.24</sub> Fe <sup>3+</sup> <sub>0.18</sub> )Σ=2.98	O <sub>11.89</sub> OH <sub>0.11</sub>	
<b>Antao (2013)</b>	(Ca <sub>2.964</sub> Mg <sub>0.010</sub> Mn <sub>0.026</sub> )Σ=3.000 (Ca <sub>2.960</sub> Mg <sub>0.012</sub> Mn <sub>0.028</sub> )Σ=3.000	(Mg <sub>0.083</sub> Fe <sup>3+</sup> <sub>1.608</sub> Fe <sup>2+</sup> <sub>0.006</sub> Cr <sub>0.001</sub> Al <sub>0.007</sub> Ti <sup>4+</sup> <sub>0.295</sub> )Σ=2.00 (Mg <sub>0.121</sub> Fe <sup>3+</sup> <sub>1.401</sub> Fe <sup>2+</sup> <sub>0.023</sub> Ti <sup>4+</sup> <sub>0.455</sub> )Σ=2.00	(Si <sub>2.795</sub> Al <sub>0.205</sub> )Σ=3.000 (Si <sub>2.689</sub> Al <sub>0.200</sub> Fe <sup>3+</sup> <sub>0.111</sub> )Σ=3.000	O <sub>12.000</sub> O <sub>12.000</sub>	
<b>Adamo et al. (2011)</b>	Ca <sub>3.000</sub>	(Ti <sub>0.002</sub> Al <sub>0.005</sub> Cr <sub>0.017</sub> Fe <sup>3+</sup> <sub>1.952</sub> Mn <sub>0.001</sub> Mg <sub>0.016</sub> )Σ=1.993	Si <sub>3.008</sub>	O <sub>12</sub>	
<b>Locock et al. (1995)</b>	(Ca <sub>2.866</sub> Mn <sub>0.019</sub> Mg <sub>0.080</sub> Na <sub>0.038</sub> )Σ=3.003	(Mg <sub>0.055</sub> Mn <sub>0.013</sub> Fe <sup>2+</sup> <sub>0.057</sub> Fe <sup>3+</sup> <sub>0.631</sub> V <sup>3+</sup> <sub>0.014</sub> Al <sub>0.137</sub> Ti <sup>4+</sup> <sub>1.058</sub> Zr <sub>0.039</sub> )Σ=2.004	(Si <sub>2.348</sub> Fe <sup>3+</sup> <sub>0.339</sub> Fe <sup>2+</sup> <sub>0.311</sub> []) <sub>0.005</sub> Σ=3.003	O <sub>12</sub>	
<b>Chakhmouradian and McCammon (2005)</b>	(Ca <sub>2.899</sub> Mn <sub>0.020</sub> Fe <sup>2+</sup> <sub>0.058</sub> Na <sub>0.023</sub> )Σ=3.000	(Mg <sub>0.156</sub> Fe <sup>2+</sup> <sub>0.197</sub> Fe <sup>3+</sup> <sub>0.556</sub> Al <sub>0.049</sub> Ti <sub>0.959</sub> Zr <sub>0.080</sub> Nb <sub>0.003</sub> )Σ=2.000	(Si <sub>2.302</sub> Al <sub>0.171</sub> Fe <sup>3+</sup> <sub>0.497</sub> []) <sub>0.030</sub> Σ=3.000	O <sub>11.880</sub> OH <sub>0.120</sub>	
<b>Antao (2014)</b>	(Ca <sub>2.91</sub> Mg <sub>0.05</sub> Mn <sup>2+</sup> <sub>0.03</sub> )Σ=2.99	(Ti <sub>1.09</sub> Fe <sup>3+</sup> <sub>0.46</sub> Fe <sup>2+</sup> <sub>0.37</sub> Mg <sub>0.08</sub> )Σ=2.00	(Si <sub>2.36</sub> Al <sub>0.14</sub> Fe <sup>3+</sup> <sub>0.51</sub> )Σ=3.01	O <sub>12</sub>	
<b>Novak and Gibbs (1971)</b>	(Ca <sub>2.96</sub> Mn <sub>0.04</sub> )Σ=3.00	(Al <sub>1.95</sub> Fe <sub>0.05</sub> )Σ=2.00	Si <sub>3.00</sub>	O <sub>12</sub>	
<b>Schingaro et al. (2001)</b>	(Ca <sub>2.97</sub> Ba <sup>2+</sup> <sub>0.03</sub> )Σ=3.00	(Mg <sub>0.11</sub> REE <sup>3+</sup> <sub>0.02</sub> Zr <sup>4+</sup> <sub>1.12</sub> Ti <sup>4+</sup> <sub>0.68</sub> Fe <sup>3+</sup> <sub>0.07</sub> )Σ=2.00	(Si <sub>1.33</sub> Al <sub>0.81</sub> Fe <sup>3+</sup> <sub>0.85</sub> )Σ=2.99	O <sub>12</sub>	
<b>Scordari et al. (1999)</b>	(Ca <sub>2.75</sub> Mg <sub>0.05</sub> Mn <sup>2+</sup> <sub>0.07</sub> Fe <sup>2+</sup> <sub>0.13</sub> )Σ=3.00	(Ti <sup>4+</sup> <sub>0.04</sub> Ti <sup>3+</sup> <sub>0.12</sub> Fe <sup>3+</sup> <sub>1.12</sub> Fe <sup>2+</sup> <sub>0.05</sub> Al <sub>0.67</sub> )Σ=2.00	(Si <sub>2.88</sub> Ti <sub>0.05</sub> Fe <sup>3+</sup> <sub>0.04</sub> )Σ=2.97	O <sub>11.83</sub> OH <sub>0.17</sub>	

**Table 8.** Comparison of refined bond distances (Å) and mean atomic numbers (electrons, e<sup>-</sup>) of cation sites as determined by structure refinement (X-ref) and EPMA for the studied crystals. Average error on mean atomic number ± 0.5 e<sup>-</sup>.

	<b>W6</b>	<b>W12</b>	<b>W16</b>	<b>NZALA</b>	<b>ZER2</b>
<b>Y-O</b> <sub>X-ref</sub>	2.008(1)	2.008(1)	2.010(1)	2.0121(4)	2.009(1)
<b>Y-O</b> <sub>EPMA*</sub>	2.014	2.015	2.018	2.022	2.017
<b>Y-O</b> <sub>EPMA**</sub>	2.025	2.019	2.026	2.032	2.030
<b>Z-O</b> <sub>X-ref</sub>	1.684(1)	1.671(1)	1.681(1)	1.6615(4)	1.656(1)
<b>Z-O</b> <sub>EPMA*</sub>	1.696	1.669	1.687	1.666	1.648
<b>Z-O</b> <sub>EPMA**</sub>	1.692	1.666	1.689	1.665	1.650
<b>m.a.n.(X)</b> <sub>X-ref</sub>	20.00	20.00	20.00	20.00	20.00
<b>m.a.n.(X)</b> <sub>EPMA*</sub>	19.66	19.99	19.66	19.89	19.93
<b>m.a.n.(X)</b> <sub>EPMA**</sub>	19.98	20.07	19.95	19.97	20.07
<b>m.a.n.(Y)</b> <sub>X-ref</sub>	22.50	22.52	22.46	23.31	23.30
<b>m.a.n.(Y)</b> <sub>EPMA*</sub>	23.48	23.31	23.22	24.01	24.13
<b>m.a.n.(Y)</b> <sub>EPMA**</sub>	22.84	23.76	23.30	24.39	24.05
<b>m.a.n.(Z)</b> <sub>X-ref</sub>	15.85	14.75	15.74	14.61	14.00
<b>m.a.n.(Z)</b> <sub>EPMA*</sub>	15.95	14.99	16.20	15.18	13.74
<b>m.a.n.(Z)</b> <sub>EPMA**</sub>	16.06	14.51	15.74	14.87	13.66

*Note:* \*according to our cation distribution; \*\*according to the Grew et al. (2013) cation distribution.